8439

NAME OF AUTHOR...Baird,.George.A................................

TITLE OF THESIS..The.fast.neutron.intensity.at.high.altitude.

....

....

UNIVERSITY.......of.Calgary..............................

DEGREE FOR WHICH THESIS WAS PRESENTED......Ph.D,............

YEAR THIS DEGREE GRANTED...1966...~~(1965)~~...............

Permission is hereby granted to THE NATIONAL LIBRARY

OF CANADA to microfilm this thesis and to lend or sell copies

of the film.

The author reserves other publication rights, and

neither the thesis nor extensive extracts from it may be

printed or otherwise reproduced without the author's

written permission.

(Signed)...*George A. Baird*......

PERMANENT ADDRESS:

..83.Weston.Pk........

..Drumcondra..........

..Dublin.14...........

DATED..3.Apr.........1971

UNIVERSITY OF ALBERTA AT CALGARY

'THE FAST NEUTRON INTENSITY AT HIGH ALTITUDE'

by

GEORGE A. BAIRD

A THESIS

SUBMITTED TO THE FACULTY OF GRADUATE STUDIES

IN PARTIAL FULFILMENT OF THE REQUIREMENTS FOR THE DEGREE

OF DOCTOR OF PHILOSOPHY

DEPARTMENT OF PHYSICS

CALGARY, ALBERTA

OCTOBER 1965

UNIVERSITY OF ALBERTA AT CALGARY
FACULTY OF GRADUATE STUDIES

        The undersigned certify that they have read, and

recommend to the Faculty of Graduate Studies for acceptance, a

thesis entitled 'The Fast Neutron Intensity at High Altitude',

submitted by George A. Baird in partial fulfilment of the

requirements for the degree of Doctor of Philosophy.

_____
                      Supervisor

_____

_____

_____

_____

Date: _OCTOBER 27, 1965_____

(ii)

ABSTRACT

A neutron detector, using pulse shape discrimination in anthracene, has been developed and used to measure the neutron flux and energy spectrum at high altitude and high latitude. The characteristics of the detector are discussed.

The differential neutron energy spectrum determined at residual pressures of less than 0.1 gm/cm^2 at 68.8° geomagnetic north, may be approximated by

$$\frac{dN_n}{dE_n} = 0.30 \pm 0.06 \ E^{-0.7 \pm 0.3} \ \text{neutrons}/cm^2\text{-sec-MeV}$$

The spectrum at atmospheric depths, 200 - 600 gm/cm^2, is given by $kE^{-1.4 \pm 0.3}$ neutrons/cm^2-sec-MeV.

The results, discussed in context with other experiments, give a latitude effect which is in good agreement with the theoretical change predicted by Lingenfelter (1963), and are not inconsistent with his free space flux values in the region 1 to 10 MeV. The form of the spectrum at 0.1 gm/cm^2, showing an appreciable exponent change from data obtained lower in the atmosphere, is in fair agreement with the predictions of Newkirk (1963) and provides support for the conclusions of Boella et al (1965) derived from balloon experiments.

ACKNOWLEDGEMENTS

The author would like to thank:

Dr. B. G. Wilson, who supervised the experiment, for his continuing interest in the project and for much valuable discussion during the writing of this thesis.

Dr. J. R. Prescott for several informative discussions about 'neutrons in organic scintillators'.

Drs. C. D. Anger and T. A. Clark for help with the balloon programme.

Mr. W. L. Haney and the Space Electronics Section of the National Research Council for the essential part they played in the preparation and launch of the rockets.

Dr. G. C. Nielson for the use of the Van de Graaff at the University of Alberta, Edmonton.

Mr. C. Hanson and Mr. D. Will who contributed greatly to the design and calibration of the detector respectively.

Mr. R. H. Johnson who coded and debugged the Monte Carlo programme.

Mrs. L. Coulthard who assisted with the typing.

My wife, who typed most of the manuscript from the author's illegible scrawl and who proof read the final copy.

The University of Alberta at Calgary and the National Research Council, for their financial support in the form of Graduate Teaching Assistantships, Scholarships and Summer Grants.

TABLE OF CONTENTS

LIST OF TABLES

LIST OF ILLUSTRATIONS

CHAPTER 1

INTRODUCTION

The cosmic ray neutron is a secondary particle produced by the interaction of a primary cosmic ray with a nucleus of the atmosphere. This interaction is commonly referred to as a nuclear star. The neutron in the free state is an unstable particle with a half life of approximately 1000 seconds, the decay reaction being given by

$$n = p^+ + e^- + \nu \, .$$

However, very few of the neutrons produced in the atmosphere live long enought to decay, the majority being absorbed by atmospheric nuclei. Between its birth in a nuclear star and its death in a beta decay or absorption, lies the interesting life of a cosmic ray neutron.

In the following chapter the production and loss of neutrons will be discussed. In this section a brief life history of the cosmic ray neutron will be given.

When a high energy cosmic ray primary strikes an 'air' nucleus, the reaction can be very complicated, and the attempted explanations can be found in any cosmic ray text [e.g. Cranshaw (1963)]. As the details of the reaction are not directly related to this work, a more simplified approach will be taken. If a nucleon with energy in excess of 200 MeV hits an air nucleus, the products of the interaction will almost certainly include a group of 'knock-on' or 'prompt' particles, shot out

of the nucleus along the line of flight of the incoming primary
particle. The primary itself may be among these particles
having lost only half or so of its energy in the collision.
The knock-on particles formed in this manner will have various
energies, but in general only one particle will have an energy
of the same order as the incident particle. The knock-on
particles typically escape from the nucleus in 10^{-22} seconds.

The 'residual' nucleus, left behind after the escape of
the knock-on particles is excited and will normally de-excite
by the emission of 'evaporation' nucleons. The evaporation
process is not associated only with excited residual nuclei,
but also with 'compound' nuclei formed by the absorption of a
medium energy neutron (1 to 100 MeV). The neutrons from an
evaporation process have typically a Maxwellian distributed
energy spectrum centered at a few MeV. The evaporation neutrons
have a typical escape time of about 10^{-15} seconds.

As the neutron is uncharged it can lose energy only by
direct collisions with the nuclei of the atmosphere. The
knock-on neutrons, if they have energies in excess of 100 MeV,
may cause further 'knock-on' type stars and can effectively
produce more evaporation type stars until the energy falls
below about 10 MeV. It is also possible, if the knock-on neut-
ron was produced close to the top of the atmosphere by a par-
ticle travelling tangentially to the earth's surface, that the
neutron will escape into interplanetary space. Such a neutron
is referred to as an 'albedo' neutron. In general, however,

	Below 1 MeV	1 MeV to 10 MeV	Above 10 MeV	Total	Total
Captured to Form C^{14}	0.83	0.12	0.00	0.64	0.56
Captured by other Processes	0.04	0.51	0.90	0.19	0.31
Captured to form Tritium					0.02
Leakout of the Atmosphere	0.13	0.37	0.10	0.17	0.11
	Hess et al (1961) $\lambda = 44°N$	Hess et al (1961) $\lambda = 44°N$	Hess et al (1961) $\lambda = 44°N$	Hess et al (1961) $\lambda = 44°N$	Newkirk (1963) $\lambda = 57°N$

COSMIC RAY NEUTRON BALANCE.

Table 1

the knock-on neutrons will be directed towards the earth.

The neutrons from the evaporation stars are of too low an energy to produce more stars. The main method of degeneration of these particles is by collision with air nuclei. In this way the neutrons are reduced from several MeV to the order of KeV before either they are absorbed or decay. As the neutrons from an evaporation star have isotropic directions in the centre of mass system, a substantial number must leave the earth's atmosphere and drift into interplanetary space; hence adding to the albedo flux.

When the energy of the neutron has been reduced below 0.5 eV, by collisions, neutron capture by nitrogen becomes an important loss mechanism. The nitrogen capture leads by proton emission to carbon 14.

$$N^{14} + n \rightarrow C^{14} + p$$
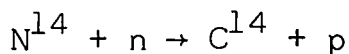
Carbon 14 is of course, the isotope measured in radioactive carbon dating. Table 1 shows a collection of the estimates of the relative numbers of neutrons lost by each of the above processes.

It will be seen from Table 1 that only about 10 to 15% of the total neutron flux leaves the earth's atmosphere by leakage (in this case 'leakage flux' and 'albedo flux' are identical: i.e. the flux leaving the atmosphere).

On the basis of an albedo neutron flux Singer (1958) predicted that there should be geomagnetically trapped radiation. This was subsequently found by Van Allen (1958). Several

authors attempting to further develop Singer's theory were hampered by a lack of data on albedo neutron flux and energy spectrum.

In this thesis an attempt has been made to determine the variation of neutron flux and energy spectrum with altitude at high geomagnetic latitude. The specific intention was to determine the albedo neutron flux and energy spectrum at solar minimum.

A review of the theoretical and experimental background to the work is given in Chapter 2. The experimental methods used by other authors are discussed in Chapter 3 and a detailed discussion of the theory, design and calibration of the present detector is presented in Chapters 4,5 and 6. The performance of all ten detectors; (See Table 7, Pages 94 and 95) 6 of which were flown in rockets and 4 of which were balloon borne; is reviewed and the results of the successful flights are analysed in Chapter 7. The energy spectrum and flux determined by these flights are compared with the results of other workers in Chapter 8.

CHAPTER 2

THEORETICAL AND EXPERIMENTAL BACKGROUND

2.1 Cosmic Ray Neutron Source

In Chapter 1 is has been seen that cosmic ray neutrons may
be divided into two groups, evaporation and knock-on neutrons.
Simpson (1951) in one of an important series of papers showed
that about 90% of the cosmic ray neutrons were produced by
evaporation stars. He also showed that the excitation energy
in these stars was on average greater than 300 MeV. Lingenfelter
(1963) deduced an energy spectrum for the evaporation spectrum
given by

$$N(E)dE = kE \exp(-E/\theta)dE \qquad (1)$$

where E is the neutron energy, $N(E)$ is the number of neutrons
produced per second in the range E to E + dE, k is a constant
and θ is the nuclear 'temperature'. Lingenfelter chose a value
of 1 MeV for θ to agree with the results for the neutrons
evaporated from carbon, excited by 190 MeV protons [Gross
(1956)], and with the theoretical calculation of Le Couteur
(1952).

The prompt or knock-on neutrons form about 10% of the
total neutron production. They have significantly different
properties from those of the evaporation neutrons. The basic
differences are in the form of the energy spectrum and the
angular distribution of the product particles.

Camerini et al (1950) have measured the proton spectrum

from cosmic ray stars in emulsions and their data have been
analysed by several authors, in terms of neutron production.
On the assumption that neutron and proton spectra have the same
form at energies greater than 50 MeV, Hess et al, (1959) der-
ived a spectrum

$$N(E) = k'E^{-2} \exp(-160E^{-2})dE \qquad (2)$$

with the same notation as used in equation 1. Wentworth and
Singer (1955) have used this data in a slightly different
manner to determine a neutron yield per interaction per MeV of
$8E^{-1.8}$.

2.2 Loss of Cosmic Ray Neutrons

Neutrons are lost from the atmosphere by two principal
mechanisms: (1) absorption by the atmosphere, and (2) leakage
from the atmosphere. The relative importance of the two mech-
anisms is tabulated in Table 1. While the calculations of
Newkirk (1963) and Hess et al (1959) are not in complete agree-
ment, the general loss mechanisms appear clear.

The loss due to capture by nitrogen is the predominant
loss mechanism in both of the above results. The value quoted
by Hess et al. yields a global average for the C^{14} source of
2.9 C^{14} atoms/cm^2/sec, which is higher than any other determ-
ination. Newkirk's result, on the other hand, yields a value
of a global average value of 2.1 C^{14} atoms/cm^2/sec, which is
lower than previous determinations. Newkirk quotes Craig (1957)
as suggesting that the value , determined from the radiocarbon

distribution, should be about 1.8 C^{14} atoms/cm^2/sec.

The loss due to leakage between the two calculations is also in disagreement. Newkirk suggests that this difference is due to the different altitude variations used in the calculations. Hess et al (1961) extrapolated their results by means of an exponential to the top of the atmosphere. Newkirk, however, took into consideration the transition maximum. This would indicate that the calculation of Newkirk was indeed a better approximation.

As a general conclusion, it is safe to assume that at middle latitudes approximately 85 to 90% of the neutrons produced are eventually absorbed by the atmosphere. The remaining 10 to 15% form the leakage or albedo flux.

2.3 The Equilibrium Energy Spectrum

The neutron energy spectrum in the atmosphere depends, not only on the production spectrum, but also on the energy loss mechanism. The energy loss mechanism for neutrons is a purely nuclear collision process. The neutrons of higher energy may, as outlined previously be absorbed to form stars, hence producing more neutrons, i.e. inelastic collisions; or at lower energy they may simply bounce off the nucleus losing some energy to it, i.e. an elastic collision. It is difficult to obtain an analytic expression for such processes and detailed calculations of the equilibrium flux had to await the advent of high speed computers. For this reason the original work on the

neutron energy spectrum was mainly experimental.

Early work on the energy spectrum was carried out mainly by Yuan (1951) and Simpson (1951). Experiments were performed using boron triflouride counters and the neutrons were arbitrarily separated into 'fast' and 'slow' neutrons by the detecting apparatus. These data, along with predictions from the data of Camerini et al (1950) lead to a quite accurate determination of the differential neutron energy spectrum below the transition maximum (approximately 100 gm/cm^2). The data obtained by Miyake et al (1957) between 1 and 15 MeV, from a hydrogen filled cloud chamber, agrees very well with the spectrum deduced by Yuan.

The most complete experimental data on the energy spectrum is due to Hess et al (1959), which was analysed in more detail by Hess et al (1961). The energy spectrum was measured by a set of detectors effectively covering the energy range from thermal energies to about 1 GeV. The results showed for the first time the existence of a maximum at about 1 MeV in the energy spectrum, corresponding to the evaporation source spectrum (See Figure 2-1). It will be seen from Figure 2-1 that there is also a maximum at low energies. This is due to the absorption of lower energy neutrons by nitrogen.

Of the more recent experiments, few have been able to determine accurately the shape of the spectrum over such a wide range, though most experiments agree with Hess et al (1961) within the limits of accuracy (e.g. Bame et al (1963)). The

experiments of Mendell and Korff (1963) and Haymes (1964) were able to determine the spectrum over the range 1 to 14 MeV. Their results give a spectrum which follows an $E^{-1.3}$ law at high altitude, in reasonable agreement with the results of Hess et al.

Theoretical calculations on the expected energy spectrum depend quite strongly on the source spectrum used. Hess et al found that the evaporation source spectrum has the most pronounced effect on the final neutron spectrum. While their results do not agree very well with the calculations of Newkirk (1963) in the region above 1 MeV, they are in close agreement below this energy (Figure 2-1).

The data on the differential spectrum at altitudes less than 60,000 ft may then be summarized as follows: -

1. The shape below 1 MeV, as shown in Figure 2-1 is well known and can be approximated from 100 KeV to 1 MeV by an $E^{-0.9}$ law (Newkirk (1963)).

2. The position and relative size of the maximum at approximately 1 MeV is open to some doubt, as is the shape of the curve following the maximum.

3. There is a maximum at about 0.1 eV due to the absorption of neutrons by the nitrogen in the atmosphere at lower energies.

2.4 The Altitude Variation of the Neutron Distribution

The isotropic distribution of evaporation neutrons,

AUTHOR	Simpson, 1949	Soberman, 1956	Lord, 1950	Gauger, 1962		
DETECTOR	$B^{10}F_3$ Moderated 1.75 inches	$B^{10}F_3$ Unmoderated	Stars in Emulsion	$B^{10}F_3$ Moderated 2 inches		
ATMOSPHERIC DEPTH IN GM/CM^2	270	"Equilibrium" Region *	"Equilibrium" Region *	170	210	230
L IN GM/CM^2	157	164	165	165	132	127

VALUES OF THE ABSORPTION MEAN FREE PATH

Table 2

* The values of L quoted by Soberman and Lord were calculated for the entire 'equilibrium' region, i.e. an unspecified distance below the transition.

together with the relatively short (~ 90 gm/cm^2) thermalization mean free path, suggests that neutrons detected at any point must have been produced close by. It would be expected therefore that altitude variations would closely parallel variations in the 'star production'. In fact the source distribution used by Lingenfelter (1963) was based on the altitude dependence of 3 and 5 pronged stars, measured by Lord (1951). Calculations, however, as with the energy spectrum, have been preceded by experiment.

Some of the earliest surveys were carried out by Yuan (1951) and Simpson (1951). Simpson showed that the altitude variation could be represented by an exponential function

$$N \propto \exp(x/L)$$

where x is the atmospheric depth and L the absorption length or mean free path. Gauger (1963) has however shown that L is not constant throughout the atmosphere but increases with altitude. Several determinations of L are compared in Table 2.

At altitudes greater than about 200 gm/cm^2 there is a maximum, the transition maximum, in the neutron intensity, the position of the maximum depending on the latitude. At still higher altitudes the variation with height becomes more complex and appears to be energy dependent.

At thermal energies the flux falls by at least a factor of 10 from the transition maximum to the extrapolated top of the atmosphere (Miles (1964), Haymes (1959)). For E > 1 MeV, Haymes (1964) finds only a factor of 4. This smaller value is

LATITUDE VARIATIONS	ALTITUDE	DATE	THEORY OR EXPERIMENT	AUTHORS
1:4.2	40 gm/cm^2	1956	E	Soberman 1956
1:7	Leakage 0 gm/cm^2	Solar Max	T	Lingenfelter 1963
1:12	Leakage 0 gm/cm^2	Solar Min	T	Lingenfelter 1963
1:4.5		1951	E	Simpson 1951
1:3.0	0 gm/cm^2	1962	E	Trainor and Lockwood 1964
1:2.5	680 gm/cm^2	1958-60	E	Pomerantz and Agarwal 1962
1:1.8	Sea Level	1956	E	Rose et al 1956
1:13	All altitudes up to 15 gm/cm^2	1964	E	Greenhill et al 1965

LATITUDE VARIATIONS AT VARIOUS ALTITUDES

Table 3

corroborated by Mendell and Korff (1963) over the same energy range, but at higher latitude. On the other hand, Bame et al (1963) in the energy range 0.1 to 10 MeV find a larger value.

In comparing the theoretical calculations of Newkirk (1963) and Lingenfelter (1963) with his own results, Haymes shows that the derivation by Newkirk is a better approximation especially at the highest altitudes.

At very high altitudes, 300 km, the altitude variation has been determined as $R^{-3.2}$, where R is the altitude expressed in earth radii (Hess and Starnes, 1960).

2.5 The Latitude Variation of the Neutron Distribution

The latitude variation of the energetic neutron flux at sea level is well known from neutron monitor measurements (Rose et al, 1956; A.E. Sandström et al, 1962). The variation at higher altitudes however, is not as well understood. Surveys at high altitudes have been made by Simpson (1951), Soberman (1956), Pomerantz and Agarwal (1962), Hess et al (1959), Bame et al (1963), Trainor and Lockwood (1964), Gauger (1963), Williams and Bostrom (1964), Lockwood et al (1965), and Greenhill et al (1965). The total latitude variation from the equator to the poles, from several of these experiments, is listed in Table 3, along with the theoretical value of Lingenfelter (1963). Several of the experiments [e.g. Gauger (1963), Lockwood et al (1965)] were confined to a limited range of latitudes and are not included in the table.

From a survey of the available data it is apparent that the
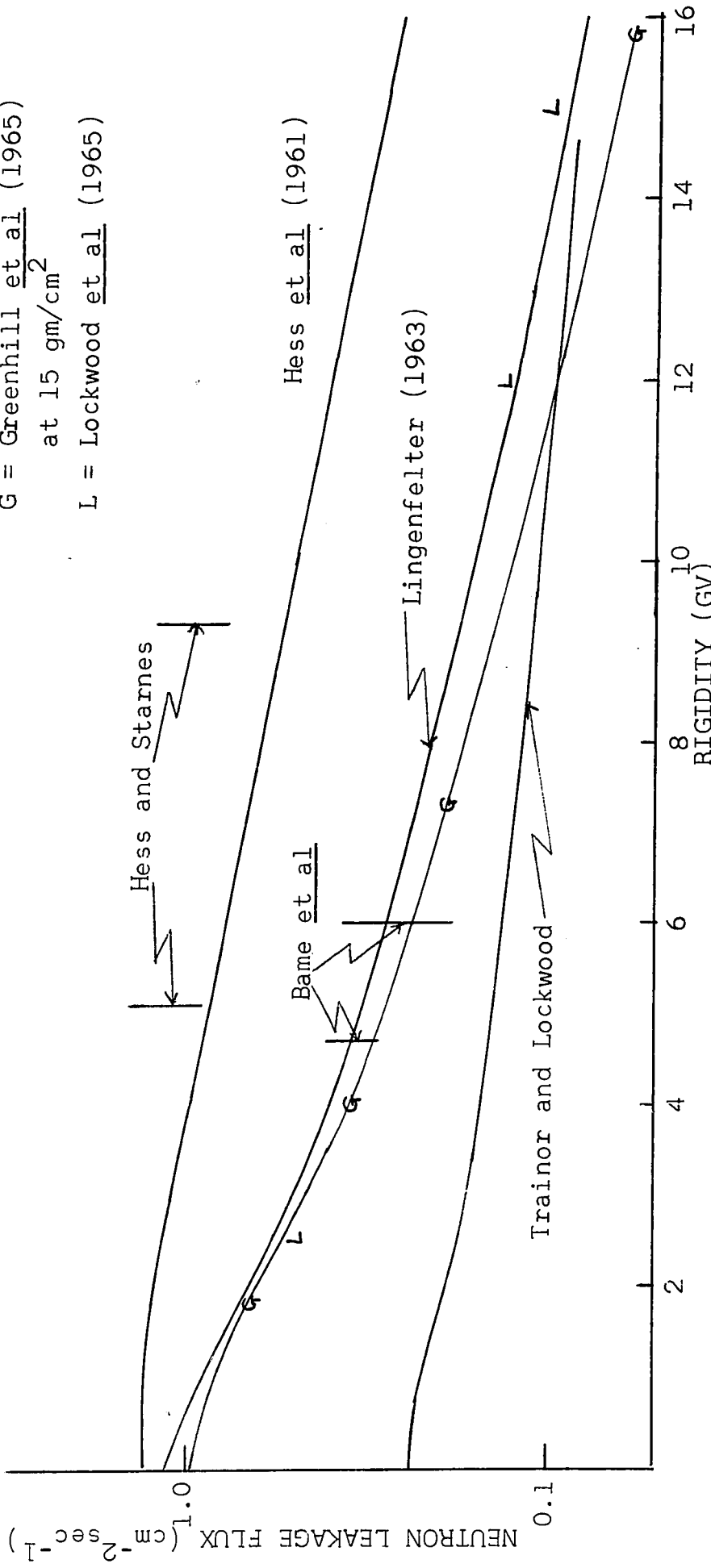
NEUTRON LEAKAGE FLUX AS A FUNCTION OF RIGIDITY FROM GREENHILL ET AL (1965)

Figure 2-2

latitude variation is altitude dependent, the low altitude values being in general smaller than those at high altitude. The variation is also dependent on the time of the solar cycle, as might be expected. The recent determinations by Greenhill et al (1965), Bame et al (1963), Lockwood et al (1965), appear to agree much better with the calculations of Lingenfelter (1963) than with the previous determination by Trainor and Lockwood (1964). Despite other inconsistent results, it appears at this time that, at solar minimum, the leakage neutron flux shows a total latitude variation of about 1:12 between the equator and the poles. Figure 2-2, taken from Greenhill et al (1965) shows the variation of the neutron count as a function of rigidity. The experimental points of Bame et al (1963) and Lockwood et al (1965) have been included for comparison.

It should be pointed out at this stage that the measurements referred to above are all essentially flux measurements with little or no spectral resolution. It has however been pointed out by Lenchek and Singer (1963) that the evaporation spectrum, and hence the equilibrium spectrum, may change with the energy of the exciting particle. This should lead to a change in the equilibrium spectrum with latitude. Boella et al (1965) appear to find such a change. Their results show that the leakage energy spectrum has relatively more high energy neutrons at high latitude than at low latitude.

A latitude dependence of the absorption mean free path has been reported by Simpson (1951), Gauger (1963) and Soberman (1956). The experiments showed that the mean free path varied from 0° to about

40°N, but remained constant from 40°N to the poles. Soberman (1956) also showed that the altitude of the transition maximum was latitude dependent, changing from 120 gm/cm^2 at 10°N to 75 gm/cm^2 at 88°N. These latter results are probably due to the change in the average energy of the primary cosmic rays with latitude.

2.6 Time Variations in High Altitude Neutron Flux

As neutrons are secondary particles generated by quite low energy cosmic rays, the evaporation neutron flux will be affected by all the cosmic ray time variations which are observable by ground based neutron monitors. In addition the neutron flux at high altitude may be affected by variations which are not obser-vable on the ground.

At high latitude and high altitude the flux will depend quite strongly on the state of solar activity at the time of the measure-ment. The effect of interplanetary magnetic disturbances on the counting rate of ground based neutron monitors is quite well known. However, the amplitude of the variation measured at ground level need not be the same as the amplitude measured at high altitude. To see the effect of such changes at high altitude, let us con-sider the amplitude of the eleven year variation.

Webber and McDonald (1964) show that the primary flux at 0.7 GV (200 MeV protons) for 1959 is down by a factor of 10 from the flux for 1956. The change measured at 4.0 GV (for 3 GeV protons), however, is only about 30%, so that the eleven year

variation is strongly rigidity dependent. The change becomes
pronounced only at rigidities less than 4.0 GV.

Protons of these lower energies are still quite effective
neutron producers, and at high altitude it is these protons which
will be responsible for a significant number of the neutrons.
The eleven year variation in the neutron intensity will therefore
be much more pronounced at high altitude than at low altitude.
The calculations of Lingenfelter (1963), based on the eleven year
variation data of Neher and Anderson (1962), are in agreement
with this prediction. At 310 gm/cm^2 and at 70°N geomagnetic
latitude, Lingenfelter (1963) finds an increase of about 25%
from cosmic ray minimum to maximum; at 0 gm/cm^2 and at 70°N
geomagnetic latitude an increase of about a factor of two from
cosmic ray minimum to maximum.

The flux of neutrons at high altitudes is therefore one of
the more sensitive indications of the state of the primary cosmic
ray flux. Extending the results given for the eleven year varia-
tion, it is obvious that the high altitude flux must also be very
sensitive to such variations as Forbush decreases, (the loss of
lower energy particles from the primary beam) and some solar flare
effects (the addition of low energy particles to the primary beam).
Both these effects have been widely studied by ground based equip-
ment. The solar flare effect in particular has recently been
widely studied by the use of riometers, which can detect the
arrival of low energy protons (< 100 MeV) in the polar region. These
protons give rise to the Polar Cap Absorption (P.C.A.) events and

may increase the neutron flux at high altitude.

Therefore, in any attempt to determine the quasi-steady state of the high altitude neutron flux, care must be taken to eliminate or allow for geomagnetic disturbances.

The picture, however, is further complicated by sporadic changes of unknown origin. Such changes have been noted by Haymes (1959, 1964), Gauger (1963), Korff and Haymes (1960), and Parsons et al (1963). The changes noted by Korff and Haymes and Parsons et al occurred during an auroral display; while changes noted by Haymes and Gauger occurred at low latitude. It is quite difficult to characterize these variations. However, from a review of the available data it appears that the occurrence of neutron increases with aurora may be fortuitous. While excess neutrons may be expected in the polar regions during PCA events, it seems unlikely that neutrons could be generated in a proton or Type A aurora. The changes, both increases and decreases, measured by Haymes (1959, 1964) at 49°N do not appear to be associated with any significant geomagnetic activity. The increase observed by Gauger (1963) appears to be due more to a shifting of the latitude knee to very low latitudes than a true increase in the count rate. In a more recent paper, Gauger (1965) found an anomalous increase in the region of the South Atlantic magnetic anomaly. From other data obtained during the same flight at approximately 30,000 feet, he suggests that the increase is associated with an increase in the night airglow.

The measured amplitude of these time variations has been up

to a factor of three above the ambient. Parsons et al (1963) in attempting to correlate the variations with x-ray and riometer data, show that for their equipment the required increase in the 100 MeV protons is too small to be measured by either of these two methods. However, Haymes (1964) shows from the simultaneous measurement of the neutron, gamma ray, charged particle and soft x-ray components, that the increase in the neutron counts was directly associated with an increase in the gamma ray counts. Both counting rates increased by a factor of about 1.5.

The relative frequency of such short term variations is difficult to access. Parsons et al (1963) discovered two such events in a total flight time of 72 hours.

CHAPTER 3

NEUTRON DETECTION

The neutron, being an uncharged particle with a very small
magnetic moment, is inherently more difficult to detect than a
charged particle. The basis of charged particle detection is the
observation of the track of ionization left by the passage of such
a particle through matter. The ionization may be observed in mat-
ter in the gas, liquid, or solid phase. In the gas phase the
ionization may be detected by the familiar discharge tube arrange-
ments, Geiger, ionization or proportional counters, or by direct
observation of the tracks in cloud chambers or spark chambers.
In the liquid phase the tracks may be observed by a scintillation
process or by a bubble chamber. In a solid the observation is
usually made by a scintillator or by a photographic emulsion.

The detection of charged particles by Cerenkov radiation
will not be discussed as this method is limited to particles with
velocities in excess of the speed of light in the material. Hence
this method is generally applicable only to very high energy
particles.

As neutrons of themselves do not cause ionization they are
undetectable by the methods listed above. This difficulty is
overcome if the neutron can be made to produce a charged particle.
The charged particle produced may be a proton or a heavier nucleus.
This is the basis of all neutron detection. Rather than discuss
in detail all the various methods of detecting the ionizing
particle, several methods of producing the ionizing particle will

be discussed and appropriate methods of detection indicated.
Attention will be focussed on the detection of neutrons in the
energy range 0.5 to 10.0 MeV.

3.1 Useful Neutron Induced Reactions

3.1.1 $B^{10}(n,\alpha)L^7$ Reaction

This reaction is perhaps the most commonly used neutron
detecting reaction. The disintegration cross-section for this
reaction is inversely proportional to the neutron velocity at
the lowest energies but deviates from this relation at a few
hundred KeV. A marked peak occurs at about 1.9 MeV. The ir-
regular form of the cross-section with energy does not however
restrict the use of this reaction as it is used basically as a
thermal neutron detector. As the Q-value for the reaction is
high in comparison to the thermal neutron energy the α-particles
produced should be peaked in energy about 1.6 MeV. This fact
is of great importance if neutrons are to be detected against
a background flux of γ-radiation. The existence of the gaseous
compound $B^{10}F_3$, which is suitable for proportional counter filling,
has contributed to the popularity of this reaction for neutron
detection. In the $B^{10}F_3$ proportional counters the electronic
bias may be set to accept only the α-particle pulses and reject
the smaller γ-ray pulses. Several cosmic ray experiments have
been carried out using $B^{10}F_3$ counters and they are being used
in the world wide neutron monitor chain. However, if any attempt
is made to measure high energy neutron fluxes, the neutrons must

be slowed to 'thermal' energies to obtain a reasonable efficiency.

The thermalization is usually accomplished by embedding the $B^{10}F_3$ counter in a block of paraffin or polyurethane. As the thermalization is a stochastic process it is difficult to determine the energy range of the neutrons being counted. The efficiency of these moderated detectors is quite low, typically of the order of 0.01%. A second and more serious objection to this type of detector in high altitude cosmic ray work is the production of neutrons by (p,n) reaction in the moderating material. It is then impossible to distinguish 'genuine' cosmic ray neutrons from neutrons produced in the moderator.

3.1.2 $Li^6(n,\alpha)T$ Reaction

This reaction has basically the same neutron detection characteristic as the $B^{10}(n,\alpha)Li^7$ reaction, except that the cross-section for thermal neutrons is only about a quarter that of the latter. The main advantage of this reaction is that Li^6I when doped with europium can be used as a scintillator, and hence can be made a more efficient slow neutron detector. A neutron spec-trometer using various thicknesses of paraffin and a $Li^6I(Eu)$ scintillator has been described by Bramblett et al (1960).

3.1.3 $He^3(n,p)T$ Reaction

The $He^3(n,p)T$ reaction is somewhat different from the reactions previously described in that tritium has no excited states. The total energy of the system, i.e. the Q-value plus the energy of the incoming neutrons, appears as the kinetic energy of the product proton and tritium. As Q for reaction is
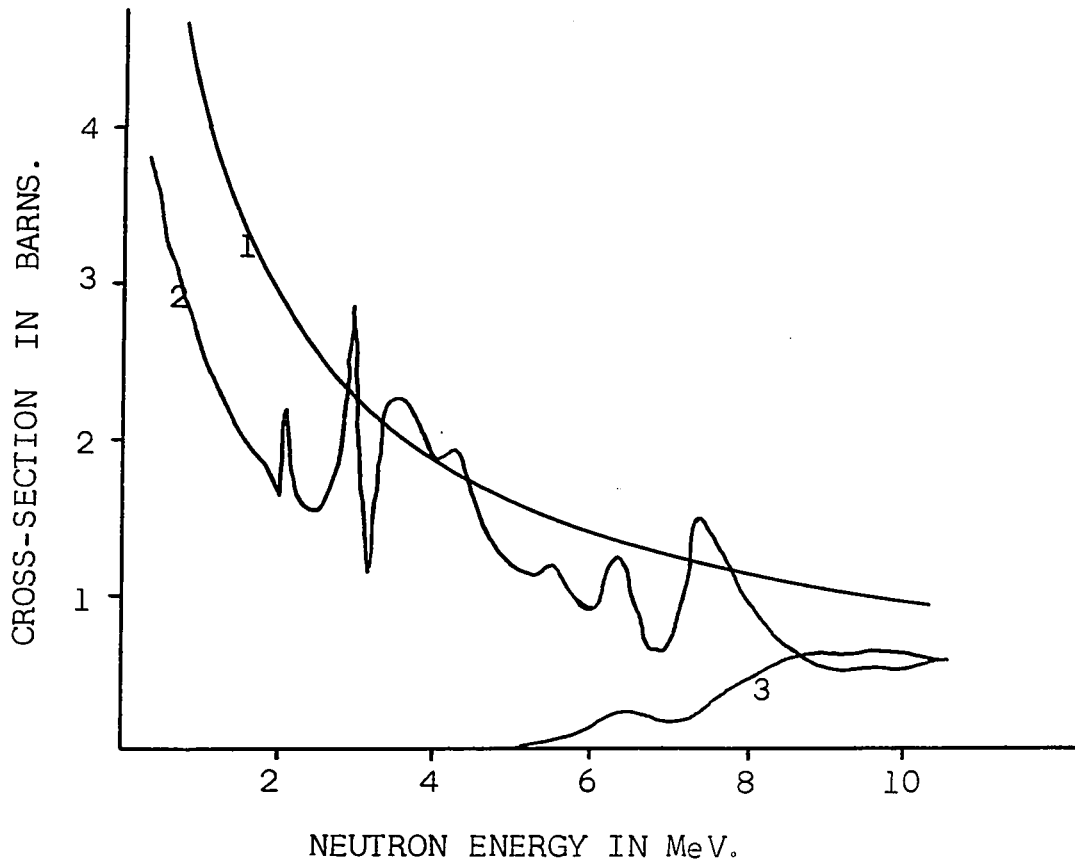
NEUTRON CROSS-SECTIONS AS A FUNCTION OF ENERGY.

1. ELASTIC COLLISIONS WITH HYDROGEN

2. ELASTIC COLLISIONS WITH CARBON

3. INELASTIC COLLISIONS WITH CARBON

Figure 3-1

known, the energy of the incoming neutron is found from $E_p + E_T - Q$, where E_p and E_T is the total energy deposited in the system. As He^3 is suitable for filling counters, this reaction is normally used in a proportional counter.

In practice it is quite difficult to derive an energy spectrum using a He^3 proportional counter due to the 'knock-on' He^3 recoils.

3.1.4 Fission Reactions

The fission of heavy atoms can be used as a neutron detecting reaction; All the fission reactions are threshold reactions. Therefore in order to obtain any information about the energy spectrum more than one detector must be used. The most widely used fission detector in cosmic ray work is the bismuth fission chamber. This chamber has a threshold of about 70 MeV.

3.1.5 Elastic Scattering

The cross-sections for elastic scattering of neutrons on hydrogen and carbon are shown in Figure 3-1. The recoil or 'knock-on' particle from an elastic scattering can be detected by almost any of the previously listed methods. However, the simplest methods are production and detection of the proton in the same material, e.g. the hydrogen filled Wilson Cloud Chamber of Miyake et al (1957) or the organic scintillators of Broek and Anderson (1960). With organic scintillators the efficiency can be made of the order of 10%. The dynamics and details of this reaction are discussed in Chapter 4.

3.2 Satellite, Rocket and Balloon Borne Neutron Detectors

The $B^{10}F_3$ proportional counter is the most popular detector
in this field. Proportional counters have been used by Trainer
and Lockwood (1964), Simpson (1951), Hess et al (1959), Bame
et al (1963), Martin (1965), Korff and Haymes (1960), and many
others. Simpson (1951), Martin, (1965), Hess et al (1959), and
Korff and Haymes (1960) all attempted to reduce the background
by using two or more similar detectors, one set boron 10 enriched,
the other set boron 10 depleted. In this way the background, due
to spurious counts, can be measured. Trainor and Lockwood (1964)
and Bame et al (1963) used moderated $B^{10}F_3$ proportional counters
to extend the energy range over which the neutrons could be counted.
Bame et al (1963) made no attempt to correct for the background
in this particular experiment. They compared their result to
a LiI(Eu) scintillator experiment to show that the background was
small. Trainor and Lockwood (1964) reduced the background by sur-
rounding the $B^{10}F_3$ proportional counters by a ring of proportional
counters. In this way any charged particle entering the paraffin
moderator will be detected by the ring of proportional counters
and gated out on the $B^{10}F_3$ counter.

Miles (1964) used the $B^{10}(n,\alpha)Li^6$ reaction in an ionization
chamber to measure the low energy neutron flux. Along with the
B^{10} ionization chamber a B^{11} loaded chamber was flown to determine
the background.

An experiment carried out by Williams and Bostrom (1964)
used solid state p-n junction detectors with a coating of B^{10}.

The twenty p-n junctions were embedded in a block of paraffin
to thermalize the neutrons; no special precautions were taken
against local production in the paraffin block.

Bramblett et al (1960) showed that it was possible by using
two different thicknesses of moderator to determine the shape of
the neutron spectrum. In their laboratory experiments they used
a $Li^6I(Eu)$ scintillator as the neutron detector. High altitude
experiments have now been conducted using this experimental ar-
rangement. The method was first used by Bame et al (1963) in
Deacon Arrow rockets and later by Boella et al (1965) in balloons.
Here again, no special precautions against local production in
the moderator were undertaken.

Hess et al (1959) and Gauger (1963) have measured the higher
energy neutron flux by means of a bismuth fission chamber. The
background is measured with a bismuth free chamber. The bismuth
chamber has a threshold at 70 MeV.

Balloon experiments by Mendell and Korff (1963) and by
Haymes (1964), have used a phoswich detector similar in nature
to the one described in this thesis. The neutron detecting scintil-
lator in both cases was NE213, the anticoincidence scintillators
were NE102 for Mendell and Korff (1963) and caesium iodide for
Haymes (1964). Both detectors are described in a Nuclear Enter-
prises Internal Report. (Reid and Hummel, March 1963). It is
felt that Haymes' detector is inherently more difficult to set
up as the neutron is detected by the middle of three time constants.
With the Mendell and Korff detector it was impossible to

discriminate between the charged particle and gamma rays; while this is not a primary requirement it is a useful check.

CHAPTER 4

ANTHRACENE AS A FAST NEUTRON DETECTOR

The philosophy behind the design of this neutron detector required a high efficiency counter with some energy resolution. In addition the detector was required to measure the small neutron flux in the presence of a proton and gamma ray flux.

The high efficiency and energy resolution requirements effectively restricted the detector choice to an organic scintillator. The presence of a proton flux required some sort of anticoincidence shield, while the gamma pulses could only be rejected by either a separate background measurement or by pulse shape discrimination. The work of Brooks (1959) showed that it was possible from the shape of the scintillator pulse to distinguish between proton and electron pulses in anthracene and stilbene. After testing the circuits of Brooks, and Daehnick and Sherr (1961) with stilbene, NE150 and anthracene scintillators, it was decided to use Brooks circuit with anthracene embedded in NE102 as an anticoincidence shield.

The reasons for this choice are as follows:

(i) Because of the three different decay times 31 ns and 53 ns in anthracene and 4 ns in NE102 it was possible with one photomultiplier to separate charged particles from gamma rays and neutrons. Stilbene was considered unsuitable as it would be impossible to separate fast stilbene (6 ns) from the NE102 pulses (4 ns), (see discussion in Section 4.4).

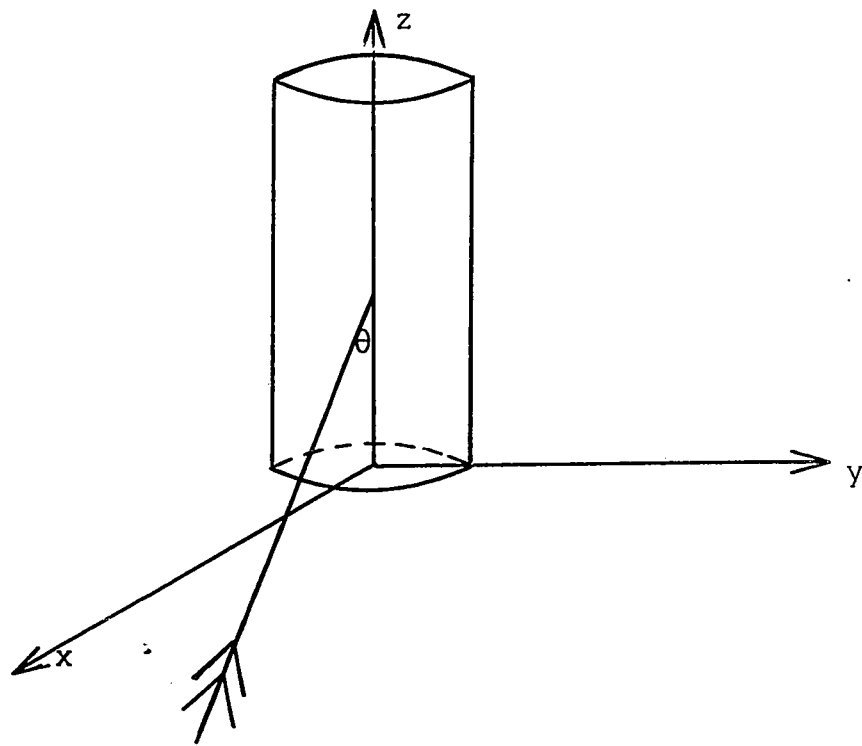(ii) As bubble free liquid scintillators were not available

SCALE 1 - 1

A

B

2"

1.5"
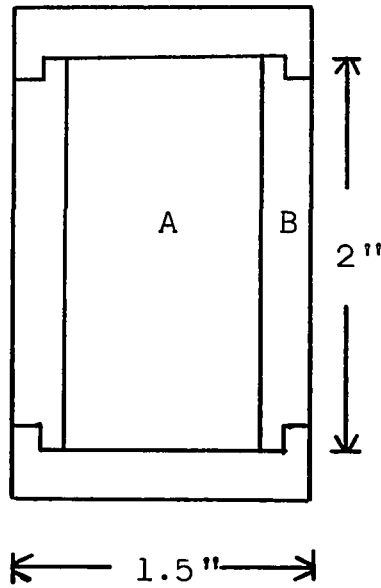
A - ANTHRACENE

B - NE102

Scale Drawing of Scintillator Arrangement

θ - ANGLE OF INCIDENCE FOR NEUTRONS
ON THE CRYSTAL USED IN MONTE CARLO
CALCULATIONS
SCINTILLATOR.

Figure 4-1

until recently, liquid scintillators were not considered suitable
for rocket flight.

(iii) The Brooks circuit proved a simpler circuit to operate
than the Daehnick and Sherr circuit, and appeared more sensitive
to the faster decay times found in anthracene.

The physical size and shape of the phosphor are shown in
Figure 4-1. All the joints were sealed with Dow Corning silicone
grease. The following sections deal mainly with the inner, anthra-
cene, crystal in which the neutrons were detected and classified.
The outer scintillator (NE102) acts purely as an anticoincidence
shield.

4.1 Efficiency for Neutron Detection

Over the range of energies 1 to 10 MeV the neutron-proton
scattering is isotropic in the center of mass system. In the
laboratory system the distribution in the scattering angle θ_1
measured from the preceding neutron direction goes as $\cos \theta_1$. If
E_o is the energy of the incident neutron then the energy of the
scattered neutron E_s is given by

$$E_s = E_o \cos^2 \theta_1.$$

The energy distribution of E_s is rectangular; consequently the
recoil proton energy is also rectangular. The proton energy
ranges, therefore, with equal probability from E_o for a head-on
collision to '0' for a glancing collision. Because of the rec-
tangular distribution in the recoil proton energy, care must be
taken over the definition of detector efficiency. It is common

practice to define the efficiency as the ratio of the number of recoil protons to the number of incident neutrons. In practice, this definition of efficiency is inadequate as the complete detecting system must have a discrimination level, so that some of the recoil protons cannot be detected. Notwithstanding, this efficiency provides a convenient starting point for further discussion.

As neutron scattering is a stochastic process it is possible for any given neutron to produce more than one recoil particle. This multiple scattering is most important at low energies and large scintillator sizes. It is also possible for the neutron to be scattered by atoms other than hydrogen. For organic crystals where the composition is basically hydrogen and carbon, scattering by carbon is not an efficient light producer. However, a neutron producing a carbon recoil may second scatter on a proton and thus produce a detectable light pulse.

The mean free path λ for neutron scattering on either hydrogen or carbon is given by

$$\lambda = \frac{1}{n_C \sigma_C + n_H \sigma_H} \qquad (3)$$

where n_C and n_H are the number of carbon and hydrogen atoms/cm^3 respectively and σ_C and σ_H are the respective cross-sections for carbon and hydrogen (see Fig. 2-3). The fraction of hydrogen collisions is then given by

$$f(H) = \frac{n_H \sigma_H}{n_C \sigma_C + n_H \sigma_H} \qquad (4)$$
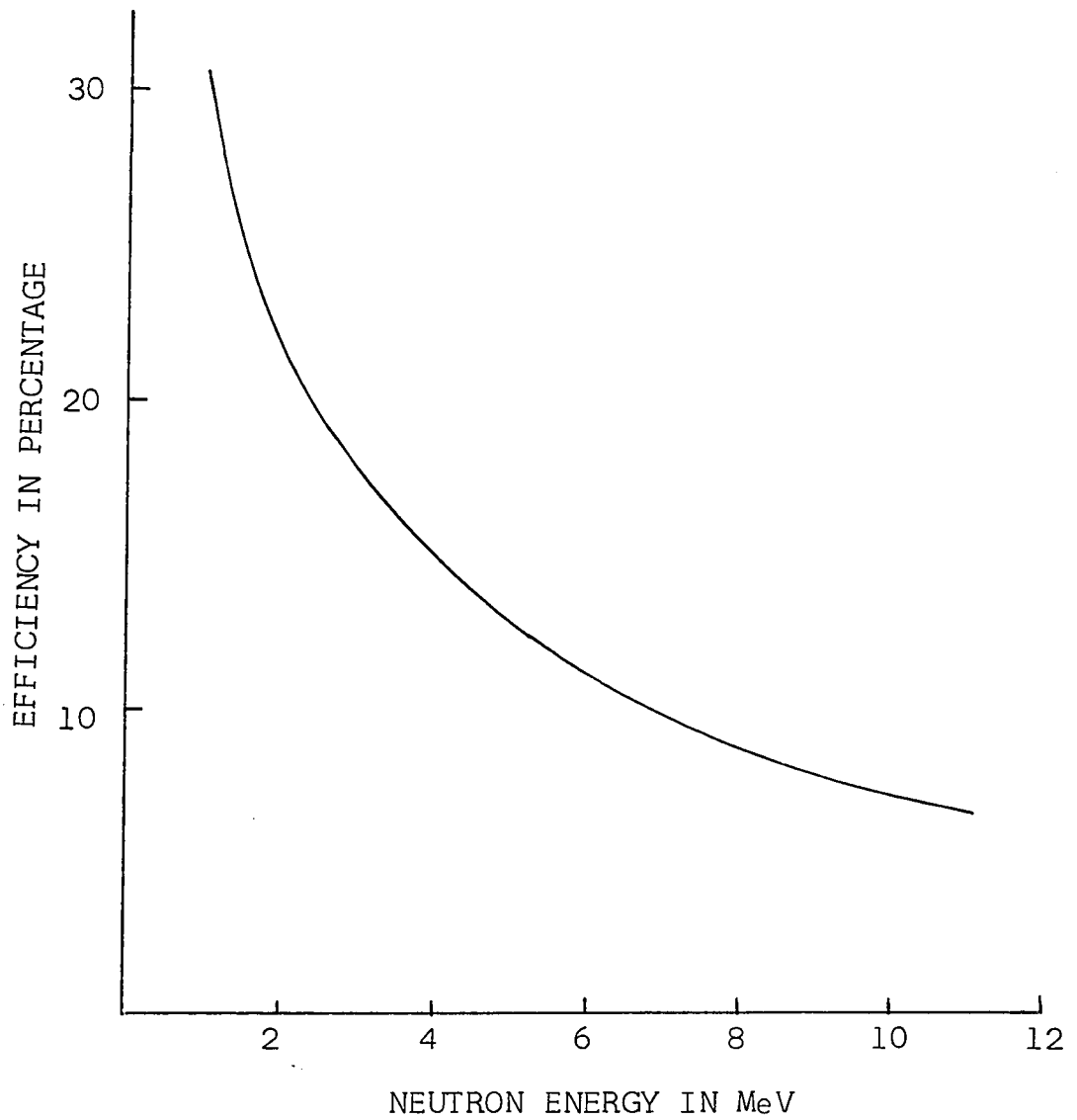
SINGLE SCATTERING EFFICIENCY FOR NEUTRONS
IN ANTHRACENE AS A FUNCTION OF ENERGY

Figure 4-2

The efficiency for single scattering is therefore given by

$$\Sigma(E,L) = f(H) \left[1 - \exp\left(-\lambda/\ell\right) \right] \tag{5}$$

where ℓ is the path length in the scintillator. The efficiency
defined in this manner is shown versus energy in Figure 4-2. As
stated previously this efficiency is misleading as it is not the
efficiency of the detector, but simply the efficiency for single
scattering on protons. In order to obtain any practical infor-
mation the light output versus the proton energy relations must
be known.

4.2 Light Output

It is well known that the light output from an organic
scintillator is not linearly related to the proton energy. This
non-linearity is perhaps the greatest drawback in the use of
organic scintillators, as a simple rectangular recoil proton
energy spectrum will not give a rectangular light output spectrum.
The most important work on this problem was done by Birks (1954)
who showed that the light output is given by

$$\frac{dL}{dx} = \frac{A \, dE/dx}{1 + kB \, dE/dx} \tag{6}$$

where A and kB are constants. For low values of dE/dx, i.e.
electrons, equation (6) may be reduced to

$$\frac{dL}{dx} \simeq A\frac{dE}{dx}$$

which gives

$$L = \int_E^0 A \, dE = AE \text{ for electrons.}$$

CAPTION FOR FIGURE 4-4

1. ELECTRONS

2. LIGHT OUTPUT CALCULATED FROM EQUATION 6
    ($kB = 0.008$ gm/cm^{2}MeV).

3. LIGHT OUTPUT USED IN MONTE CARLO CALCULATION
    (BATCHELOR ET AL. 1961).

4. LIGHT OUTPUT CALCULATED FROM EQUATION 6
    ($kB = 0.010$ gm/cm^{2}MeV).

THE EXPERIMENTAL POINTS FROM THE VAN DE GRAAFF CALIBRATION

OF DETECTORS 'B' AND 'C' ARE SHOWN AS '.',

OF DETECTOR 'A' AS 'x'.
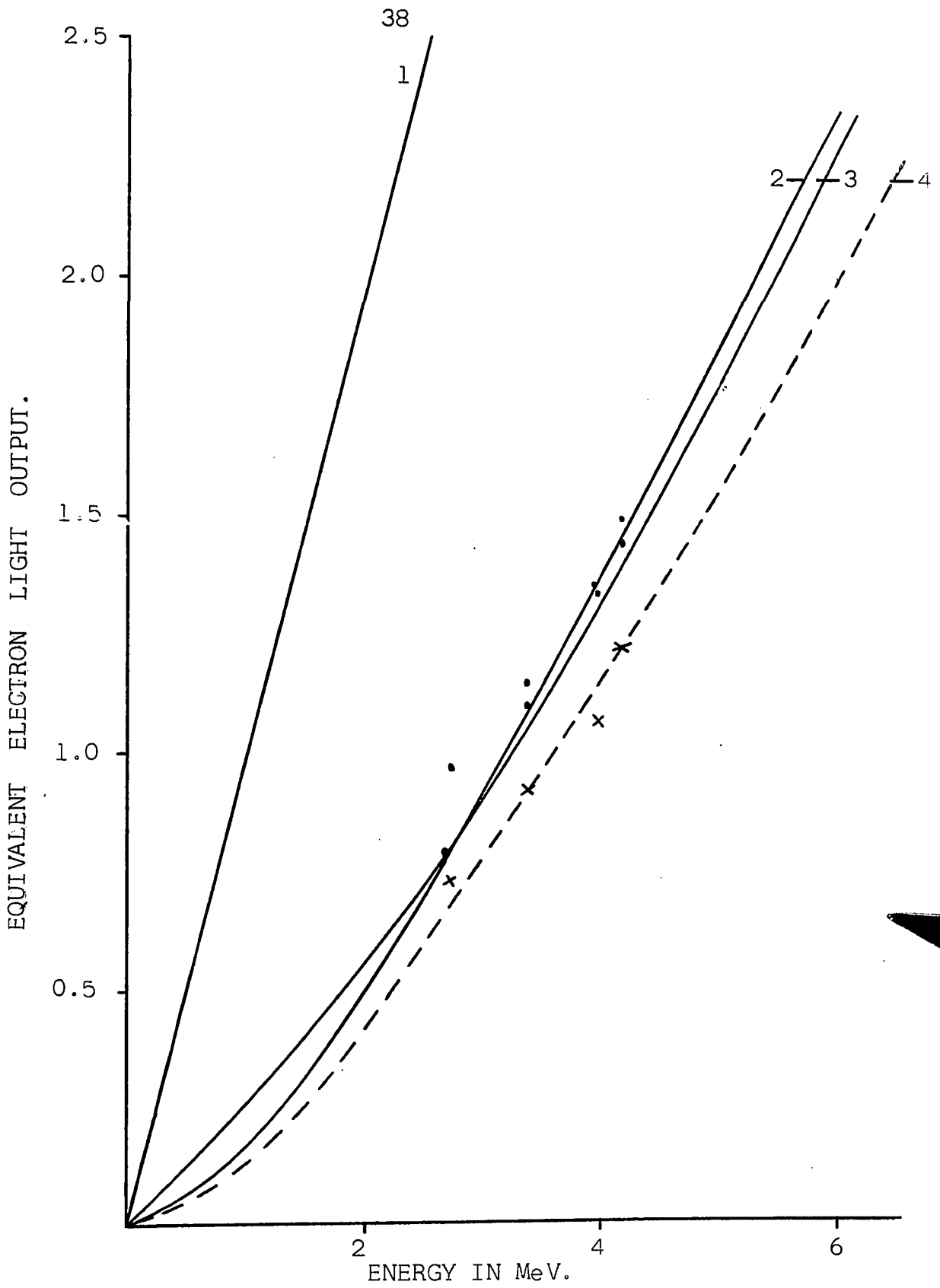
LIGHT OUTPUT RESPONSE WITH ENERGY FOR ANTHRACENE.

Figure 4-4

However, for medium values of dE/dx, i.e. protons, equation (6) becomes

$$L = \int_E^0 \frac{A \, dE}{1 + kB dE/dx}$$

For large values, i.e. alpha particles or carbon recoils we have

$$L = \int_0^R \frac{A \, dx}{kB}$$

$$= \frac{AR}{kB}$$

where R is the range of the particle under consideration.

The function $\frac{dE}{dx}$ (E) was evaluated for anthracene from the data and work of Whaling (1958). Whaling derives a 'stopping cross-section' for several elements in the atomic state and shows that the molecular stopping cross-section for a compound $X_n Y_m$ is given by

$$s(X_n Y_m) = n \, s(X) + m \, s(Y)$$

where s(X) and s(Y) are the atomic stopping cross-sections for the elements X and Y respectively. The data used in the calculation are tabulated in Table 4 and the range versus the energy curve for protons in anthracene is shown in Figure 4-3.

Having evaluated $\frac{dE}{dx}$ (E), the function $\frac{1}{1 + kB dE/dx}$ was graphed versus energy. The value of kB used was 0.00815 $gm/cm^2 MeV$. The value of A was arbitrarily set at one. The function was then graphically integrated to yield the light output in arbitrary units of electron energy. The results are shown in Figure 4-4.

4.3 The Monte Carlo Calculation of Efficiency and Light Output

The object of these calculations was to determine the light

Chemical Composition $C_6H_4(CH_2):C_6H_4$

Density of Anthracene 1.25 gm/cm^3

Molecular Weight 178.22 A.M.U.

Number of Hydrogen Atoms/cm^3 4.23×10^{22} atoms/cm^3

Number of Carbon Atoms/cm^3 5.90×10^{22} atoms/cm^3

ANTHRACENE.

Table 4.

to have hit the end of the crystal, in which case the entry co-ordinates are simpler and can be randomized according to

$$x = \Sigma_2 a \sqrt{1 - \Sigma_1^2}$$

$$y = \Sigma_1 a$$

$$z = 0.$$

In order to follow the neutron in the crystal the initial directions must also be known. The simplest method is to define the three direction cosines at entry as

$$l = - \sin \theta$$

$$m = 0, \text{ and}$$

$$n = \cos \theta.$$

4.3.2 Collision Routine

The mean free path for a neutron in anthracene is given by

$$\lambda = \frac{1}{n_H \sigma_H + n_C \sigma_C} \qquad (3)$$

The probability of losing a neutron from the beam by collision in a given interval ρ to $\rho + d\rho$ is

$$\left(\frac{dN}{N_o}\right)_\rho = \frac{e^{-\rho/\lambda}}{\lambda} \, d\rho$$

where N_o is the number of neutrons initially in the beam.

The free path of a neutron may therefore be taken as

$$\rho = -\lambda \ln \Sigma_3$$

where Σ_3 is a random number between 0 and 1. It must now be determined whether a neutron starting from point x, y, z, and travelling a distance ρ in a direction l, m, n, makes a collision inside or outside the crystal. In order to make the calculation as general as possible, this decision was made by calculating the

co-ordinates of the collision as follows

$$x' = x + l\rho$$

$$y' = y + m\rho$$

$$z' = z + n\rho$$

and comparing $x'^2 + y'^2$ to a^2 and z to h.

If the collision falls inside the crystal a decision must be made as to whether the collision was with a hydrogen nucleus or a carbon nucleus. The probability of a collision is

$$p_H = \frac{n_H \sigma_H}{n_H \sigma_H + n_C \sigma_C}.$$

The neutron therefore is considered to have hit a hydrogen nucleus if $\Sigma \leq p_H$, where Σ is a random number between 0 and 1. If $\Sigma > p_H$ the neutron is considered to have hit a carbon nucleus.

4.3.3 Hydrogen Collisions

It can be shown that the differential cross-section for elastic scattering in the center of mass system is independent of angle, i.e. the scattering is isotropic in the center of mass frame. From simple mechanical considerations it is possible to show that

$$E_s = E_o \cos^2\theta_1$$

where E_s is the energy of the scattered neutron, and θ_1 is the angle between the incident and scattered velocities in the laboratory system. As the scattering is isotropic in the center of mass system, the scattered energy will lie uniformly from 0 to E_o, hence $\cos^2\theta_1$ must be selected randomly between the limits 0 and 1. This gives the well known rectangular distribution for the knock-on proton energy from singly scattered neutrons.

In order to determine completely the direction of travel of

scattered neutrons an azimuth angle, δ, must also be chosen. The angle δ must lie between $+\pi$ and $-\pi$ and hence may be randomly chosen from $\delta = \Sigma\pi$, where Σ lies uniformly between $+1$ and -1. The direction of the scattered neutron is now completely determined in terms of $\delta, \theta_1, l, m, n, x, y$, and z.

The light output from the knock-on protons was calculated according to the equations given by Batchelor et al (1961)

$$L_p = 0.215\ E_p + 0.028\ E_p^2 \qquad (0 < E_p < 8)$$

$$= 0.60\ E_p - 1.28 \qquad (8 < E_p < 14\ \text{MeV}).$$

4.3.4 Carbon Collisions

The treatment of the carbon collisions is similar to that carried out on hydrogen. A simple scattering calculation yields

$$E_s = E_o/169\ (143 + 2\cos^2\theta_1 + 2\cos\theta_1 \sqrt{143 + \cos^2\theta_1})$$

$$\simeq E_o\ (6 + \cos\theta_1)/7$$

Since $\cos\theta_1$ can assume both positive and negative values, E_s may range from $(5/7)E_o$ to E_o.

The angular distribution was calculated from the data of Kalos and Goldstein (1956) using the equation

$$\sigma(\theta_1) = \frac{\sigma\tau}{4\pi}\ (\ 1 + 3f_1P_1 + 5f_2P_2 + \ldots\ldots)$$

$$= \frac{\sigma\tau}{4\pi}\ (1 - 2.5f_2 + 3.37f_4 - 4.06f_6)$$

$$+ (3f_1 - 7f_3 + 2.06f_5)\cos\theta$$

$$+ (7.5f_2 - 33.75f_4 + 85.3f_6)\ \cos^2\theta + \ldots$$

$$= \frac{\sigma\tau}{4\pi}\ (A + B\cos\theta_1 + C\cos^2\theta_1 + \ldots\ldots)$$

where

$$A = (1 - 2.5f_2 + 3.37f_4 - 4.06f_6)$$

$$B = (3f_1 - 7f_3 + 20.6f_5)$$

$$C = (7.5f_2 - 33.75f_4 + 85.3f_6)$$

It can be shown that B is small, so that terms in $B \cos\theta_1$ are small enough to be ignored.

It therefore follows that $\cos\theta_1$ should be distributed according to $A + C \cos^2\theta_1$.

From $\qquad \sigma(\theta_1) = \frac{\sigma\tau}{4\pi}(A + C\cos^2\theta_1)$

it can be shown that $C = 3(1 - A)$.

Therefore in order to calculate $\cos\theta$, let $x = A + C\cos^2\theta_1$ or

$dx = A \cos\theta + \frac{C}{3} \cos^3\theta_1$, where dx is a random number between 0 and 1.

This gives the required parabolic distribution for the knock-on energy between the energies $5/7E_o$ and E_o.

As with hydrogen an azimuth angle is required if we are to specify completely the direction of the scattered neutron. This azimuth angle is selected in the same manner as for hydrogen.

The light output for carbon is computed from

$$L_c = 0.017 \, E_c.$$

This light output is much less than for the same energy of proton and is in fact so low as to be generally undetectable. The importance of the carbon collision routine is the effect on the second scattering peak. In the computer programme written to carry out this analysis, the light output and the proton energy are stored in memory and the programme recycled to recalculate a new value of λ and ρ. Using the co-ordinates of the first collision as a

47
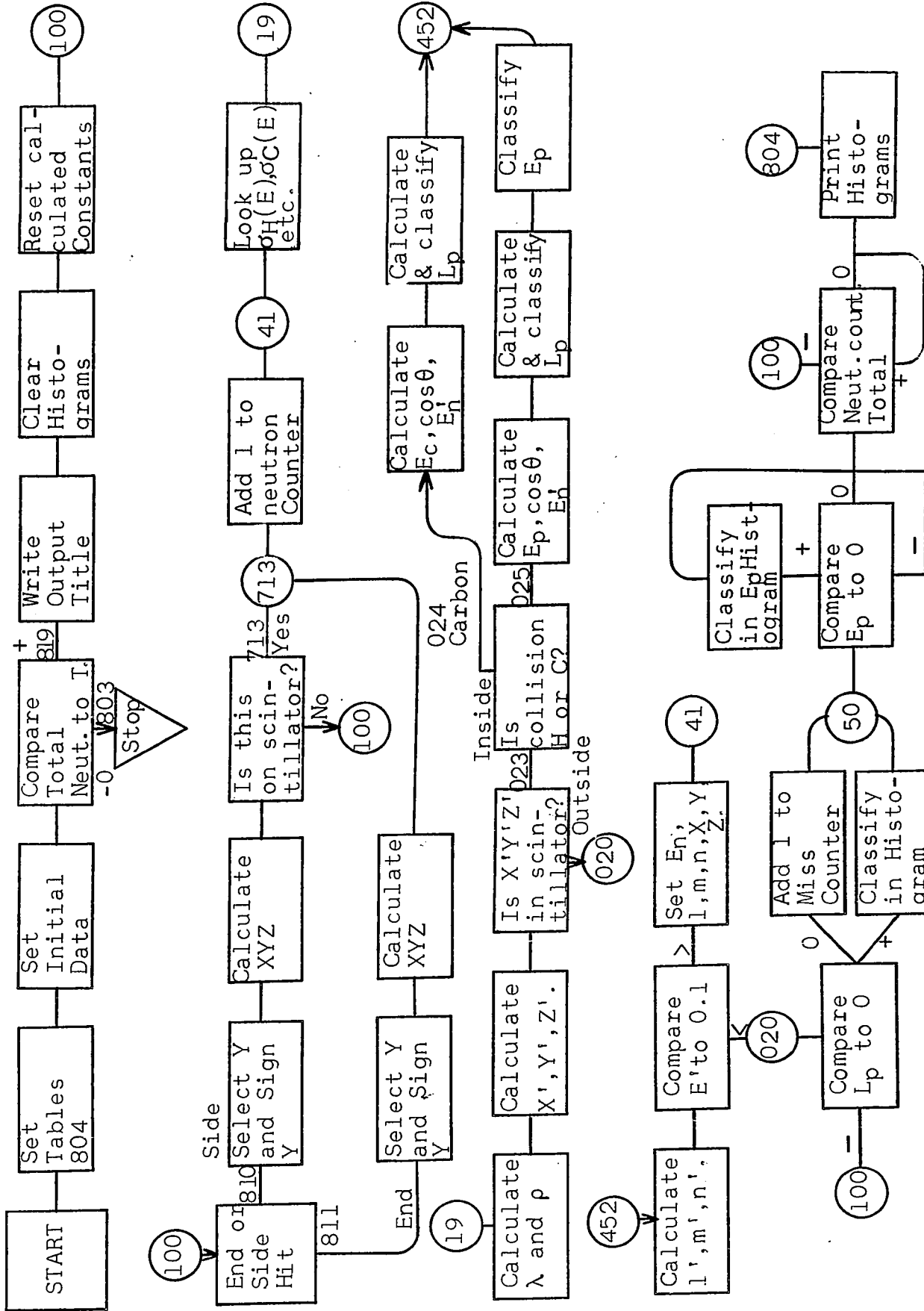
FLOW CHART FOR NEUTRON CALCULATION GENERATED BY THE COMPUTER.

Figure 4-5.

starting point, the co-ordinates of the second are calculated.
The programme then proceeds as previously described. The routine
for each neutron is terminated if the neutron escapes the crystal,
or when the neutron energy drops below 10 KeV. The accumulated
light output and proton energy are classified in their respective
histograms and the programme then selects another neutron with a
new set of entry co-ordinates. The programme is terminated when
the required number of neutrons (30,000) have been processed. The
program flow chart is shown in Figure 4-5.

4.4 Pulse Shape Discrimination

Wright (1956) working with anthracene found that the decay
time depended on the type of excitation (31 ns for beta and 53 ns
for alpha). This led several workers to construct detectors,
which, by making use of the difference in decay times, discriminated
between lightly and heavily ionizing particles. In the course of
this work it was shown by Owen (1958), and by Bollinger and
Thomas (1961), that the apparent difference in decay times was due
to differing intensities in the 'fast' and 'slow' components of
the scintillations. These workers found that the decay times for
'fast' and 'slow' components were independent of the exciting par-
ticle. The definition of 'fast' and 'slow' is somewhat arbitrary,
but a typical 'fast' decay time is of the order of 30 nsec while
the 'slow' is of the order 400 ns (Gervais de Lafond and J.
Bouyssou, 1963).

However, Falk and Katz (1962), in studying the very fast

components of the scintillation, discovered that the fast anthracene pulse was best described by

$$f(\tau) = e^{-t'/\tau_1} + Ae^{-t'/\tau_2} - (A + 1)e^{-t'/\tau_3} \qquad (7)$$

where A is a constant, t' the time from the start of the pulse and $\tau_{1\alpha}$ = 35 nsec for α-particles, $\tau_{1\gamma}$ = 28 nsec for γ-rays, τ_2 = 6 nsec for both types of radiation and τ_3 = 1 nsec. The value of attempting to define a decay time has been questioned by Walter and Coche (1962). Their results show that the decay of both anthracene and stilbene is non-exponential after about 200 nsec. The anthracene curve shows a definite break at about 400 nsec. This result agrees with the results of Gibbons et al (1961).

It is interesting to note that Walter and Coche (1962) found an exponential decay for NE102. This appears to indicate that the physical process causing pulse shape differences in anthracene and stilbene is absent in NE102.

Typical values for the percentage of light in the slow component in anthracene are 14% for protons and 4% for beta particles (Gibbons et al, 1961).

The temperature dependence of the pulse shape difference has been investigated by Brooks (1959), by Gibbons et al (1961) and by Walter et al (1963). Brooks (1959) and Gibbons et al (1961) found no change in the pulse shape effect in the range -180° to 30°C. Walter et al (1963) showed that the intensity of both 'fast' and 'slow' components changed with temperature. The changes were in the same sense and hence the total pulse shape

effect would be unaltered in the range -120° to 30°C.

Several attempts have been made to account for the pulse shape differences. The theories which gain the widest acceptance are the theory of Brooks (1959) and the modified theory of Gibbons et al (1961). Both theories depend on energy migration to retain the energy for the required time. In Brooks' theory the molecules of anthracene may be excited M^* or ionized M^+. The excited molecules may return to the ground state by

$$M^* \rightarrow M + h\nu \qquad \text{(scintillation)}$$
$$\rightarrow M + heat \qquad \text{(quenching)}$$
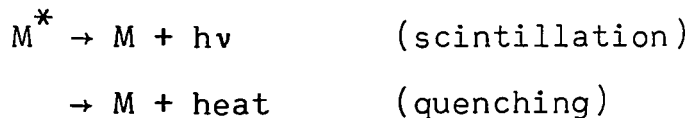
The ionized molecule M^+, however, must first recombine with a free electron before it can return to the ground state by one of the above processes. Brooks (1959) suggests that this recombination is slow and that the scintillation process is fast. Therefore an ionized molecule will tend to produce a delayed scintillation. Gibbons et al (1961) propose that the delay is caused by a M^*M^* system and they suggest that this system will have a characteristic lifetime before it decays with the release of a free exciton. These authors have predicted the loss of pulse shape effect due to impurities and the decrease of the slow component with decreasing specific energy loss. However, the existence of a pair of excited molecules is unproven.

Suhami and Ophir (1964) have shown that in practice it is not possible to discriminate between protons and electrons in anthracene until after t' = 45 nsec. This is in approximate agreement with the data of Falk and Katz (1962). However of

more general interest is the energy resolution which is possible
with this type of detector. The lowest reported proton energy
at which discrimination has been noted is 175 KeV (Owen, 1962).
At these lower energies the effect of photomultiplier noise is
one of the limiting features. The other statistical fluctuation
is in the pulse shape itself. At 175 KeV, 16% of the protons
were lost to these effects (Owen, 1962).

Suhami and Ophir (1964) have shown that the pulse shape
effect has a maximum at about 2 MeV. This result is not unexpected
as the ratio

$$\frac{dE_p}{dx_p} \Big/ \frac{dE_e}{dx_e}$$

has a maximum at this energy. The drop off from this maximum
has also been studied by Suhami and Ophir (1964).

From these results it appears that the pulse shape effect in
anthracene may be used from about 200 KeV to about 20 MeV proton
energy.

CHAPTER 5

CIRCUIT DESCRIPTION

A block diagram of the circuit is shown in Figure 5-1.
The operation of the detector depends on the pulse shape
discrimination (P.S.D.) circuit; the circuitry following the
P.S.D. circuit is a simple four channel pulse height analyser.
The high voltage power supply is an oscillator circuit feeding
a series of Cockcroft-Walton doublers. The high voltage is
regulated by a corona tube.

By way of introduction, a short general discussion of
pulse shape discrimination circuits will be given, followed by
more detailed discussion of the circuits used in the experiment.

5.1 Pulse Shape Discrimination Circuits - General

Since the feasibility of differentiating neutrons from
gamma rays in a single organic scintillator was demonstrated by
Wright (1956), the experimenter has had the choice of an ever
increasing number of pulse shape discriminating circuits.
Despite all the published circuit variations there are basic-
ally only two methods: discrimination inside the photomulti-
plier tube (space charge), and discrimination by following
circuitry. In the former case the anode is held at a potential
close to that of the dynode. During the high current phase at
the onset of a pulse, the last dynode is driven negative by the
space charge limiting between the last dynode and the anode.
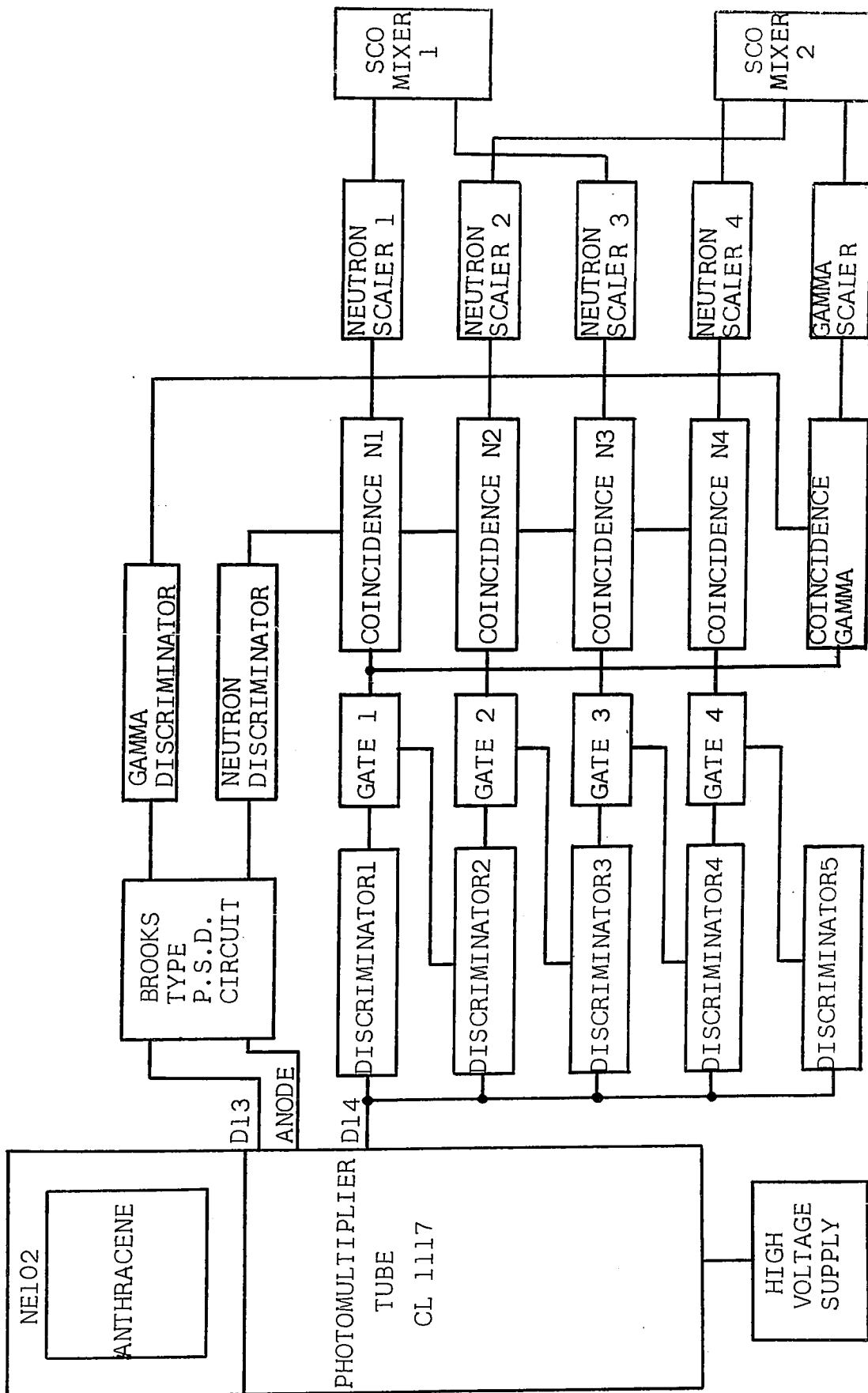
BLOCK DIAGRAM OF NEUTRON DETECTOR

Figure 5-1

5.2 Pulse Shape Discrimination Circuit by Brooks

The circuit used in this experiment is basically that
first developed by Brooks (1959). This circuit was chosen as
it could handle pulses with very small pulse shape differences,
and further, because it offered the chance of distinguishing
between three types of pulses, instead of the usual two. The
circuit requires the use of a positive and a negative pulse.
These pulses are stretched on different time constants and the
outputs compared. In the circuit used, the pulses were taken
from the 13th dynode and the anode of a 14 stage photomulti-
plier tube.

In analysing the circuits, Brooks assumed that the scinti-
llator-photomultiplier pulse was a step rise followed by an
exponential decay. If this pulse is now stretched on an RC
circuit the voltage at maximum charge is given by

$$\frac{V}{V_o} = \frac{RC}{\tau - RC}[\exp(\frac{RC}{\tau - RC}\log\frac{\tau}{RC}) - \exp(\frac{\tau}{RC - \tau}\log\frac{\tau}{RC})] \qquad (7)$$

where $V_o = Q_o/C$ or the voltage when $RC \gg \tau$

and τ = the decay time of the scintillation pulse.

This equation may be shown graphically as a function of V/V_o
and τ/RC, Figure 5-2. Let us now consider a pulse with a decay
time 'T'. The voltage produced by such a pulse depends on the
RC time constant. The dynode 13 pulse is fed into an RC
circuit with a long decay time $R_d C$, while the anode pulse is
fed into an RC circuit with a short decay time $R_a C$. The volt-
ages out of the RC circuits may be found as
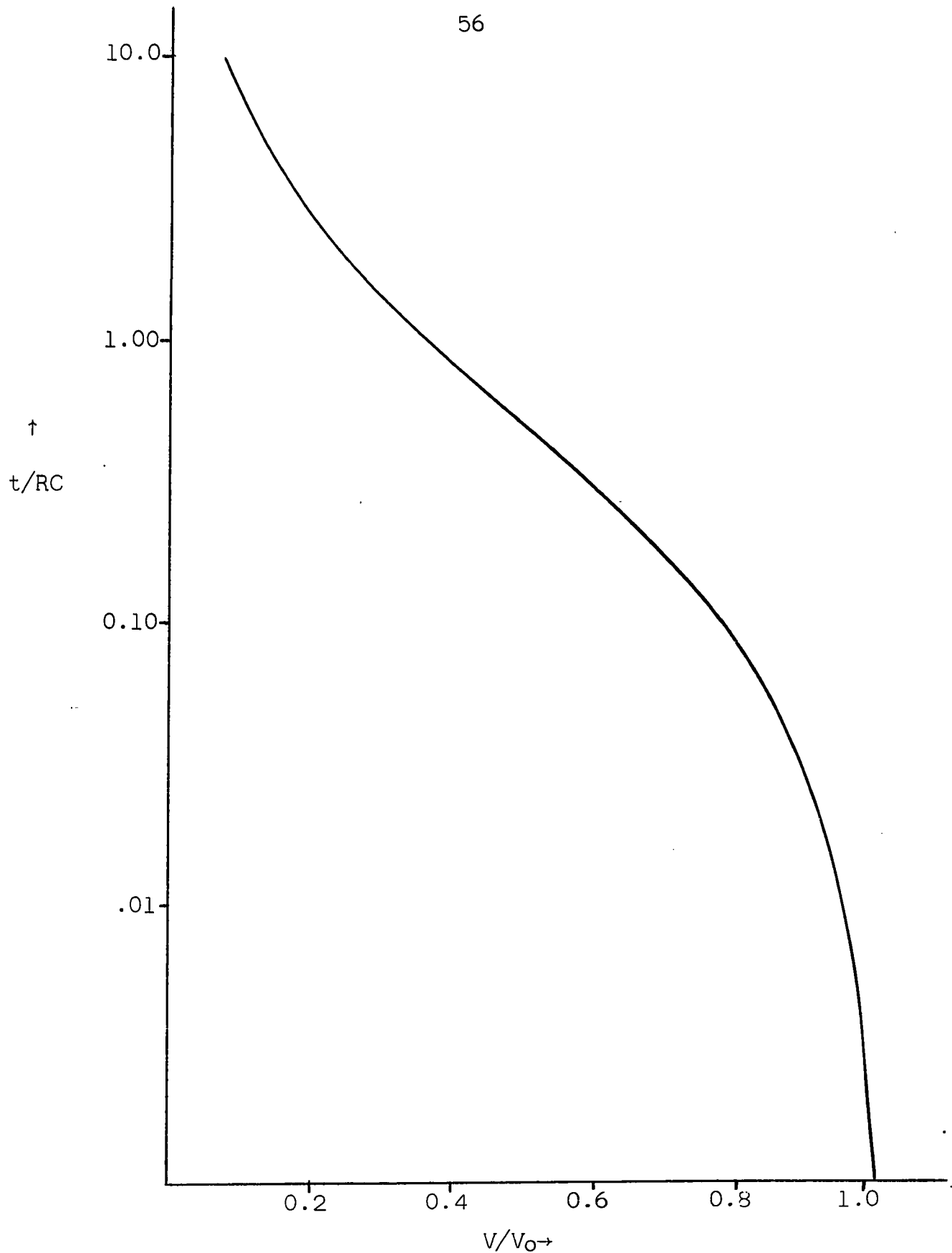
V/V$_o$ VERSUS t/RC (Equation 7)
(See Text Page 57)
Figure 5.2

$$V''/V_d = f(T_e/R_dC)$$

from Figure 5-2 and as

$$V'/V_a = f(T_e/R_aC)$$

where V_d and V_a are the anode and dynode voltages respectively

for RC $\gg \tau$.

If the gain of the photomultiplier is assumed constant

$$V_a = KV_d$$

then $\quad V' = f(T_e/R_aC).KV_d$

and $\quad V'' = f(T_e/R_dC).V_d$

If we assume that the loss in the anode circuit is ϕ_a and

that the loss in the dynode circuit is ϕ_d, it is possible, as the

anode and dynode pulses are of opposite polarity, to arrange that

$$\phi_a f(T_e/R_aC)KV_d = \phi_d f(T_e/R_dC)V_d$$

or

$$K\frac{\phi_a}{\phi_d} = \frac{f(T_e/R_dC)}{f(T_e/R_aC)}$$

This equation means that for a given set of T_e/R_dC and T_e/R_aC

values, one can arrange by selection of the current parameter

$K\phi_a$ and ϕ_d to have no net voltage output at the point B (Figure

5-3). From the graph of T/RC versus V/V_o (Figure 5-2), it can

be shown that it is possible to select T_e/R_dC and T_e/R_aC, so

that for electrons in anthracene the output is zero and for

protons, $T_p > T_e$, the output is positive.

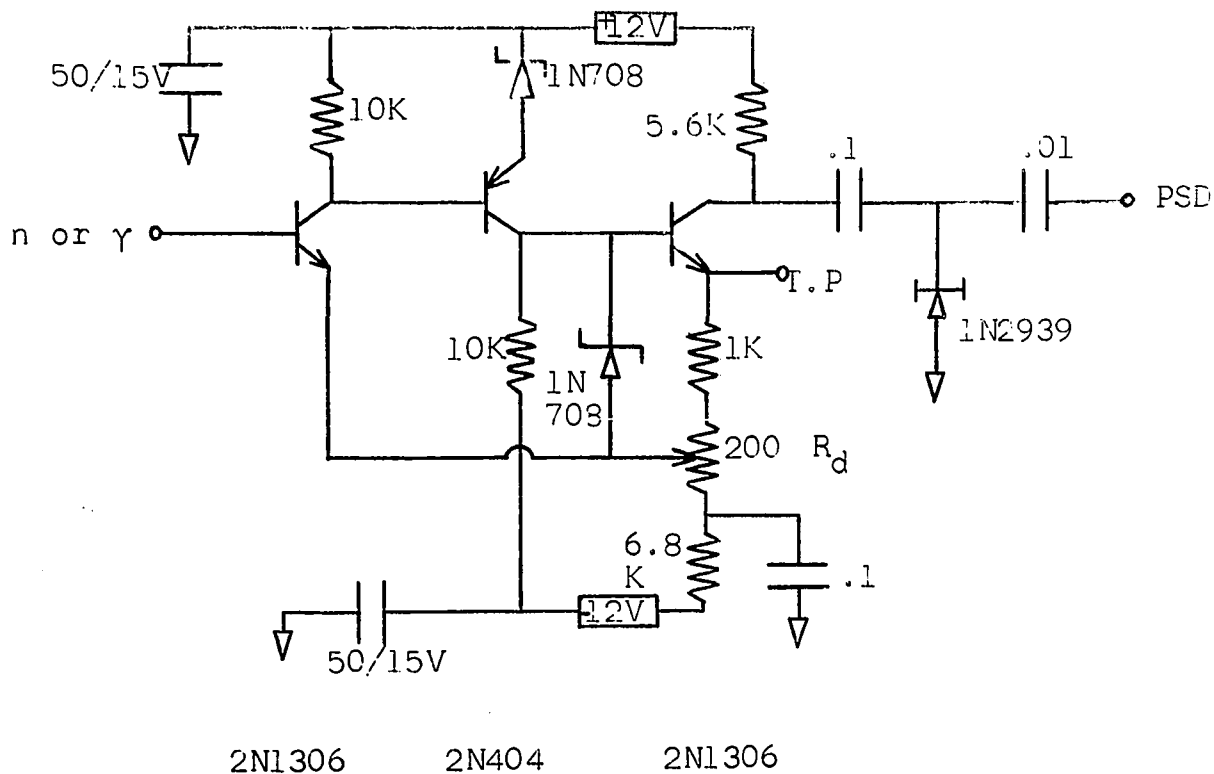In the practical circuit the pulses from the anode are

stretched on a 270Ω resistor and the photomultiplier stray

capacitance. The pulse is then fed through a gold bonded

diode, and further stretched on a 27KΩ - 150pf network. The

58

PM TUBE
BLEEDER
CHAIN

PSD CIRCUIT

R - Selected
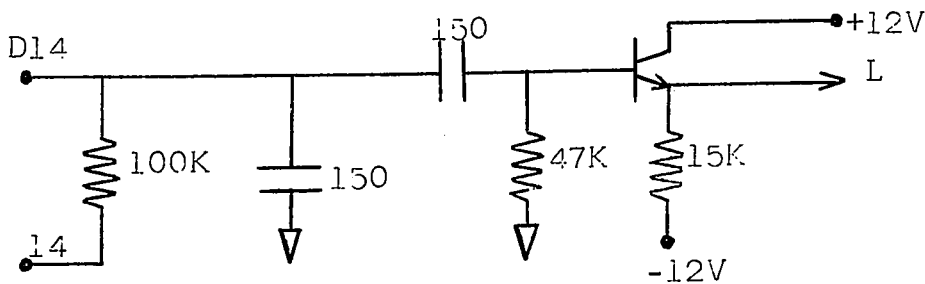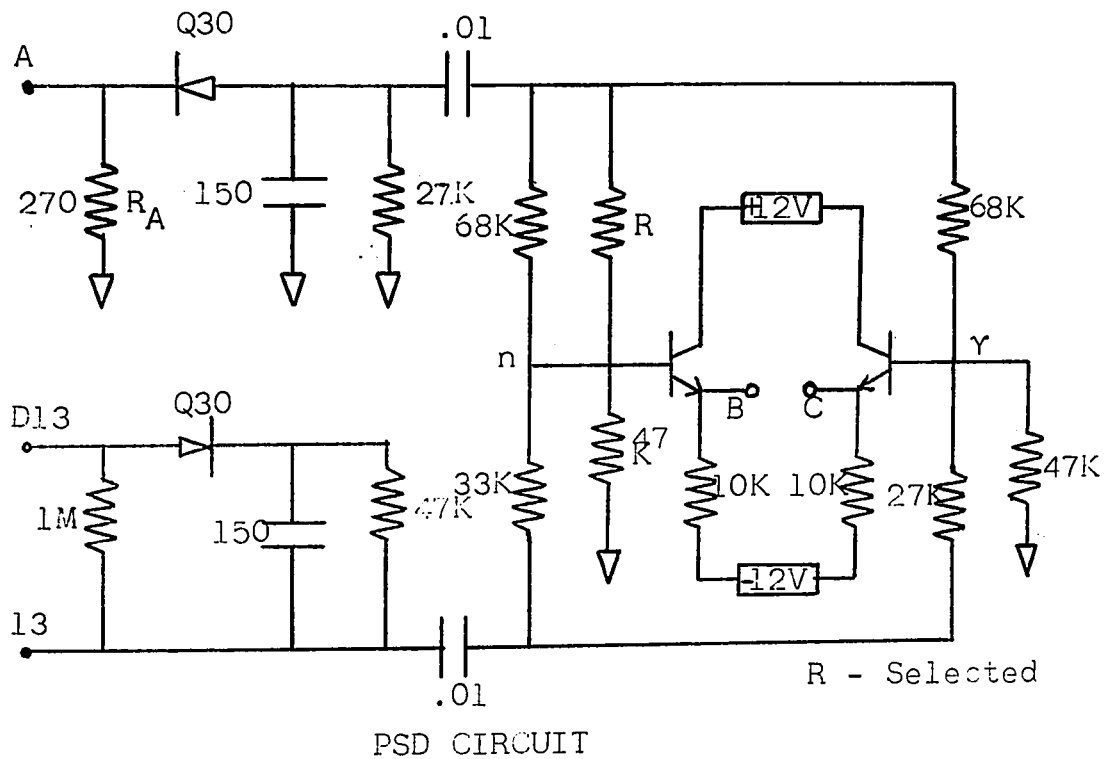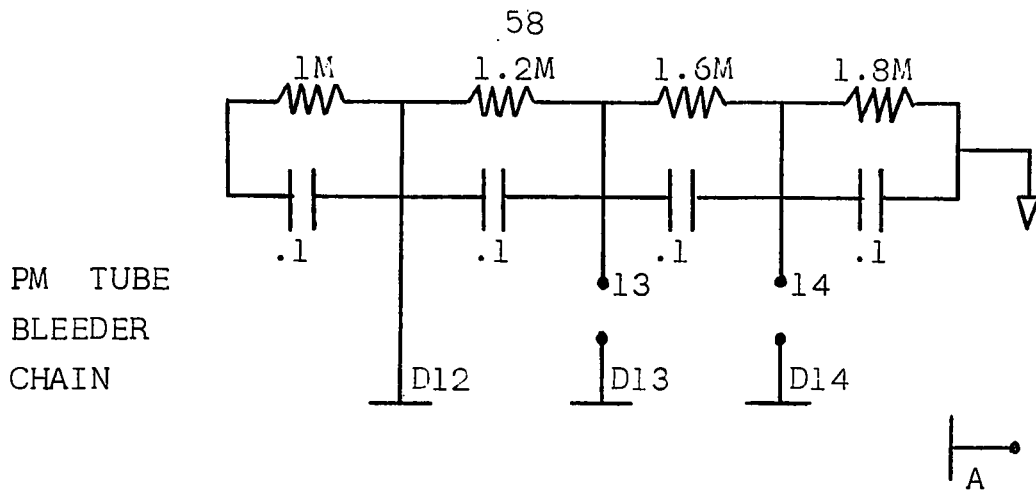
All Transistors 2N1306

LINEAR EMITTER FOLLOWER

Figure 5-3
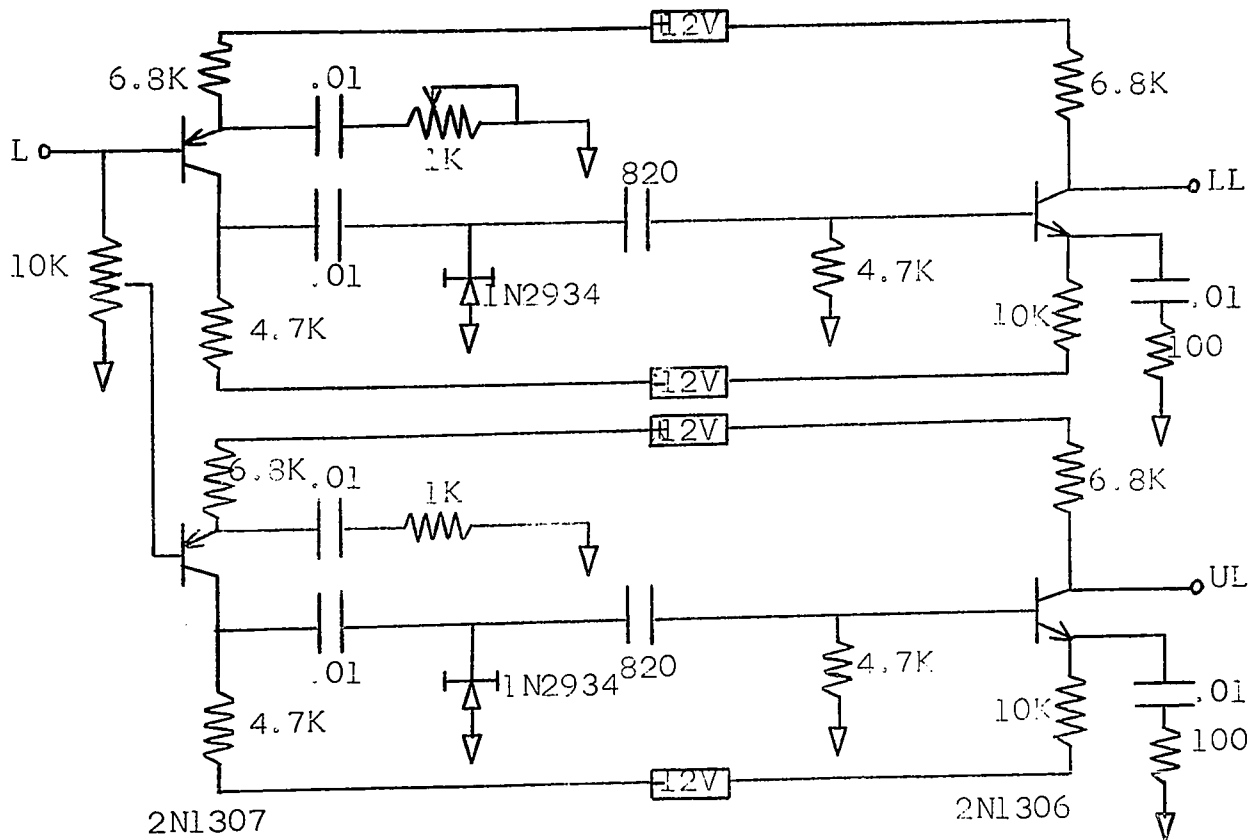
NEUTRON DISCRIMINATOR

DISCRIMINATORS

Figure 5-4

output of this RC circuit is AC coupled to the balancing

resistors, n and γ.

The dynode 13 pulses are stretched on a 1MΩ resistor and

the phototube stray capacitance. The pulse then passes through

an equivalent circuit to the anode, before it is AC coupled to

the other end of the balancing potentiometers.

For any given photomultiplier, the balancing potentiometers

and the stretching networks are adjusted to give zero output at

B for gamma rays, and zero output at C for charged particles.

Therefore a positive pulse at B corresponds to a neutron, and a

positive pulse at C to a neutron or a gamma ray (Figure 5-3).

5.3 The Neutron and Gamma Ray Discriminator (Figure 5-4)

This circuit is a tunnel diode discriminator designed to

trigger on positive pulses from the balance point B (Figure

5-3). While in theory the signal at B can be set positive,

negative or zero, the signal in practice is usually more com-

plex. In this detector, the larger signals showed a quite

significant amount of overshoot on both positive and negative

pulses. The positive overshoot from the negative pulses is un-

acceptable as the tunnel diode would interpret this as a posi-

tive pulse. To overcome this, the pulse was shaped by the

amplifier preceeding the tunnel diode, the overshoot being

removed by the limiting effect of the zener diodes.

The gain of the amplifier, and hence the discrimination
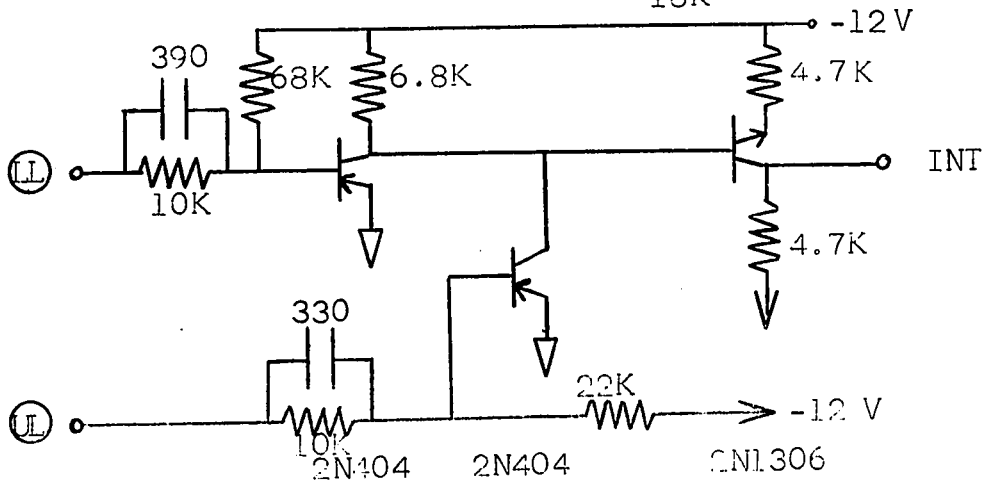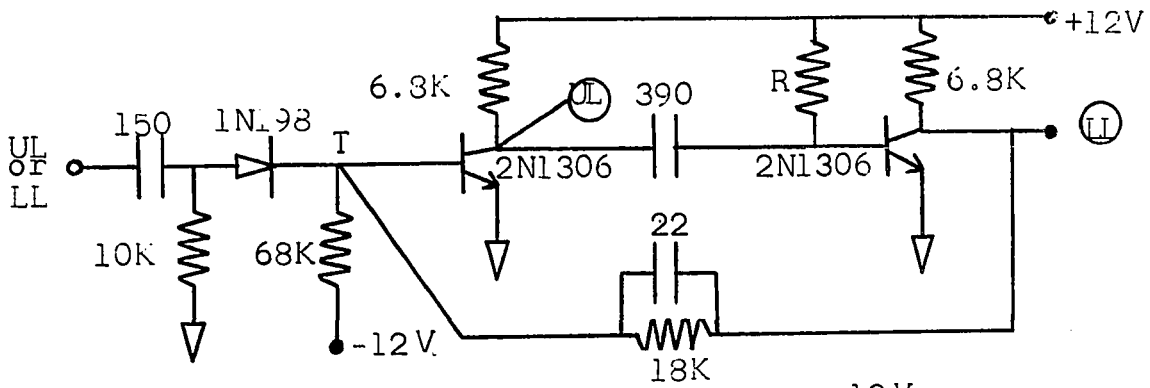
MMV AND GATE
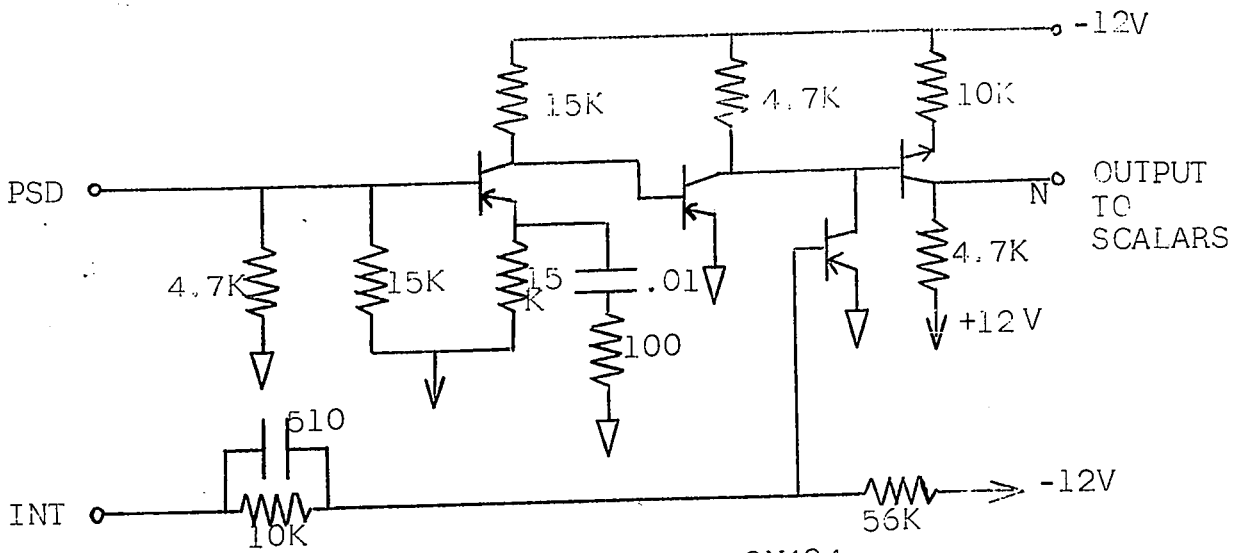
All transistors 2N404

COINCIDENCE CIRCUIT

Figure 5-5

point for the discriminator is adjusted by the resistance R_d.

The output of this discriminator is a 0.5 V negative pulse lasting approximately 1 msec.

5.4 The Pulse Height Analyser (Figures 5-4 and 5-5)

The pulse height analyser consists of a series of discriminators followed by a series of normally open gates. The pulse from the gate is then fed to a coincidence circuit, where it must be in coincidence with a pulse from the neutron discriminator before a neutron is counted.

One channel of gamma ray information was also counted as a check on the system performance. The width of the gamma ray channel varied from detector to detector.

5.5 Data Retrieval

The outputs of the coincidence circuits were fed to a series of scalers. In the rocket borne packages the outputs of two of the scaler circuits were mixed before being applied to the sub-carrier oscillator (S.C.O.) for transmission. The final record obtained after transmission was a series of d.c. level changes of two different sizes. The gamma channel was carried as a series of 15 msec spikes on one of the S.C.O.'s, each spike corresponding to a level change at the final scaler output.

In the balloon borne detectors, the outputs of the scalers were connected directly to the S.C.O.'s.

NRC HIGH VOLTAGE SUPPLY

Figure 5-6
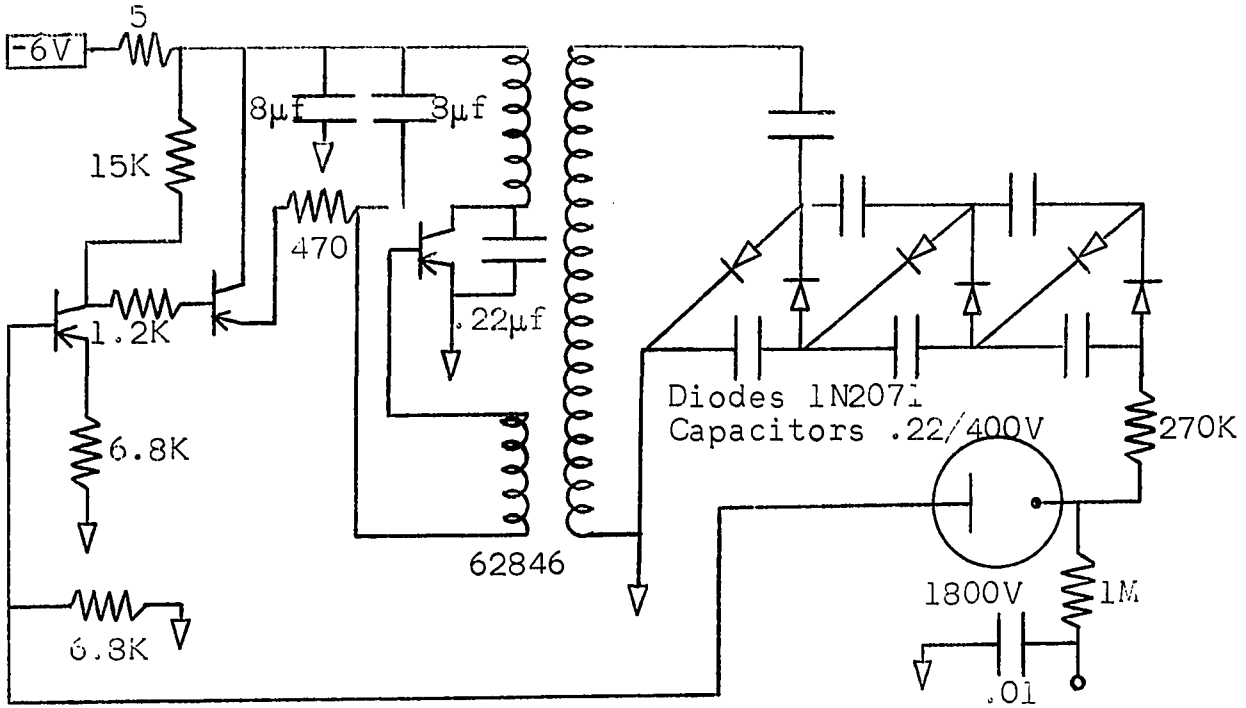
All Transistors 2N1307

BALLOON HIGH VOLTAGE SUPPLY (2)
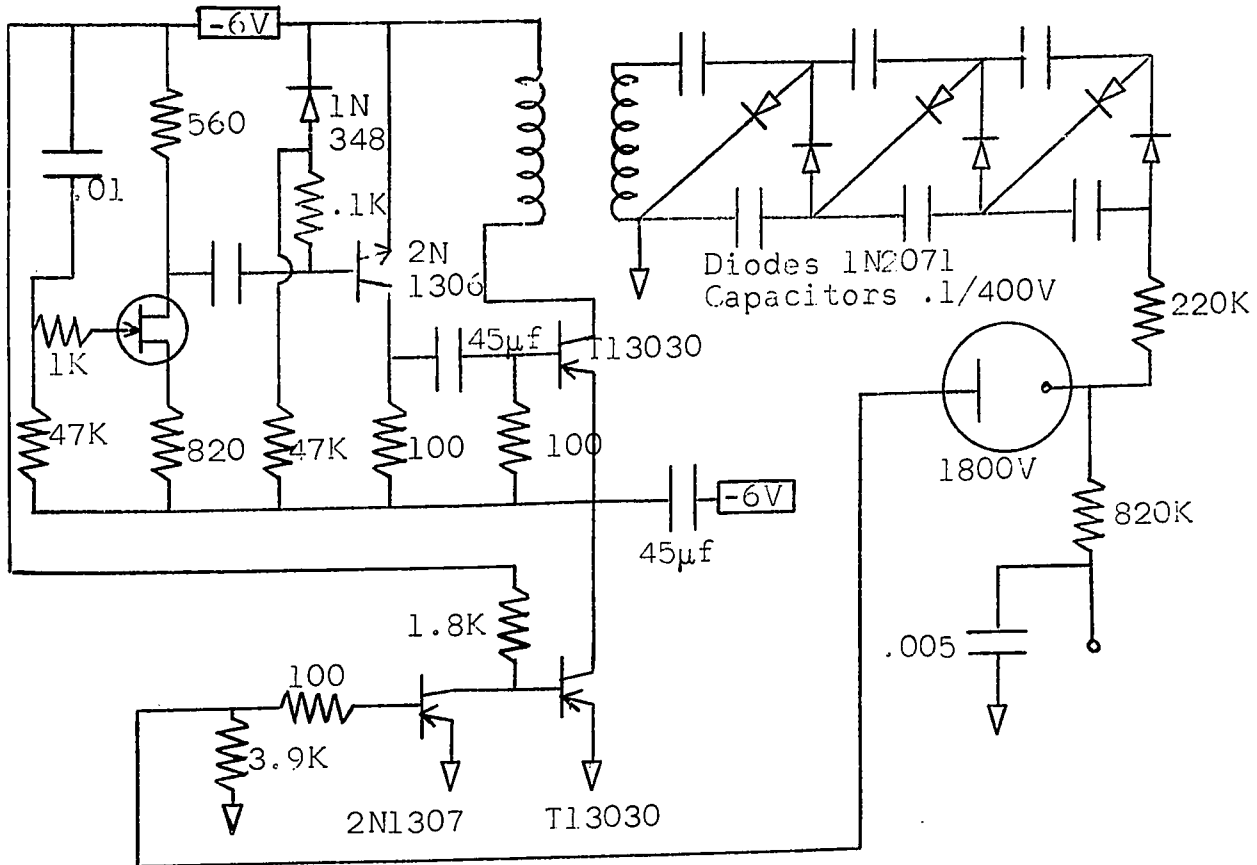
BALLOON HIGH VOLTAGE SUPPLY (1)
Figure 5-7

5.6 High Voltage Power Supply

In the rocket borne packages, a high voltage power supply, supplied by the Radio and Electrical Engineering Division of the National Research Council, Ottawa, was used. The circuit diagram is shown in Figure 5-6. The power supply was shown to have a ripple voltage of about 30 mV peak to peak at the 1920V output (Cox, private communication).

In the balloon borne packages simpler high voltage power supplies were used (Figure 5-7). These power supplies were stable to the corona tube for input voltages of 8 to 12 volts at room temperature. At very low temperatures ($-70°F$) the corona tubes themselves start to drift down in voltage. The power supplies were considered adequate over the temperature range - $30°F$ to + $70°F$. The power supply (1), shown in Figure 5-7, was an improvement over the supply (2) in Figure 5-7, in that the current requirement for the supply (1) was only about 2/3 that required for the supply (2), an important consideration for balloon flights. The noise properties of the two supplies, however, were very different. Any noise from supply (2) was in the form of single frequency (about 10 Kc) ripple, while the noise from the supply (1) was in the form of spikes. It will be seen from the circuit diagrams that the photomultiplier was operated with a grounded anode. This mode of operation was unfortunately necessary, due to the 250 mV ripple on the balloon high voltage supplies. This ripple could not be filtered out at the anode due to the stringent time constant

Eccofoam Mold Around P.M. Tube

Polyurethane Absorber

Electronic Pack
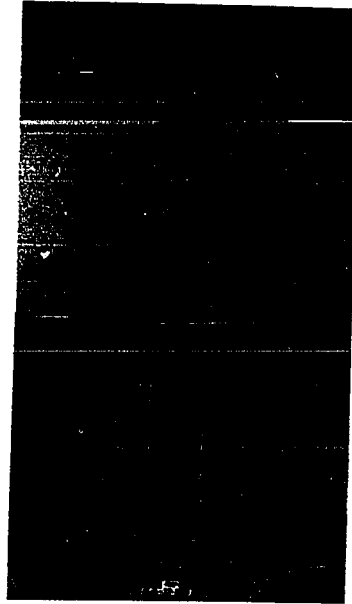
CONICAL SECTION

Electronic Circuit Boards

$\pm$ 12 Volt Zener Supply

High Voltage Power Supply

ELECTRONIC PACK

ROCKET BORNE DETECTOR

Figure 5-8

requirements of the anode P.S.D. circuits.

5.7 Enviromental Considerations

Any rocket borne detector must be able to work under large accelerations and perhaps high temperatures.

The specifications for Black Brant II require instruments to withstand 14G axial and 10G lateral accelerations. These conditions are close to the limits for the operation of fast high gain photomultiplier tubes. The only 14 stage photomultiplier able to meet these specifications was the CL1117 by the Columbia Broadcasting System. This tube was therefore used on the early rocket flights. Later the unruggedized version, the CL1004, was substituted, as the CL1117 was no longer available, and it became obvious that the accelerations were not as great as at first anticipated.

The photomultiplier was mounted very close to the nose of the rocket (Figure 5-8). The skin at this point, station 30, is normally very hot during flight, approximately 400°F. This is in excess of the melting temperature of the scintillators; also at these temperatures the photomultiplier would be very noisy and any large change in the photomultiplier noise would certainly lead to spurious results from the P.S.D. circuits. To overcome these problems, the photomultiplier μ - magnetic can was potted in about 0.5" of 'Eccofoam'; this was then surrounded by the conical Eccofoam mould shown in Figure 5-8 . The temperature at the photomultiplier on rocket, AA-II-41, did not

a higher temperature due to heat dissipation in the electronics. In fact, the detector developed corona problems before any useful idea of the self heating could be established. To avoid temperature problems, the next two balloon flights were in daylight; the temperature inside the rig did not drop below +30°F on either of these flights.

The coronal discharge due to high voltage present in a high vacuum, proved hard to solve. As previously mentioned, the scintillator and photomultiplier tube were surrounded by a μ - metal can which was maintained at the cathode potential, - 1700 to - 1900 volts. Therefore it was essential that the can and the photomultiplier bleeder chain resistors be adequately potted to prevent coronal discharge. In the eclipse flight and in flight 5 the detector was potted in Eccofoam and tested under a vacuum, 7 gm/cm^2, for 15 to 30 minutes. This was obviously not a sufficient test, as the coronal problems appeared on both flights. For flights C and 6, the high voltage parts of the detectors were first of all potted in Eccofoam, and then covered with about 0.25" of Epoxy (Eccosil). The detectors were then tested under vacuum for at least one hour. Again the detector successfully passed the vacuum chamber test, but failed in flight. No explanation of this failure can be given.

Po-Be Neutron Source
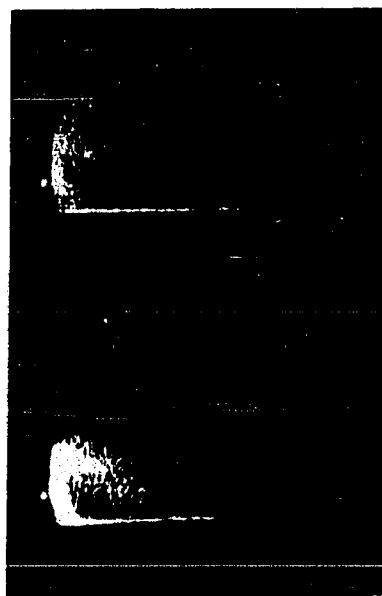
Na 22 Gamma Source

BRIGHTENING ON ALL PULSES

Extra Brightening   N2

Extra Brightening   N1

D1

Po-Be SOURCE BRIGHTENING SUPPRESSED

TWINKLE BOX DISPLAY
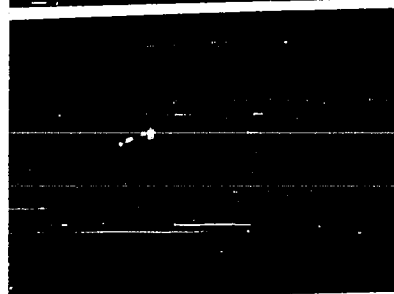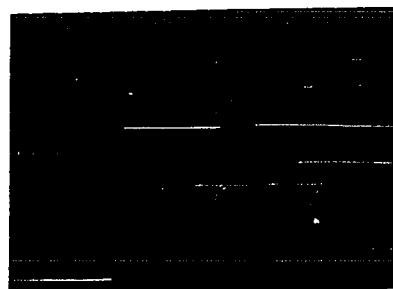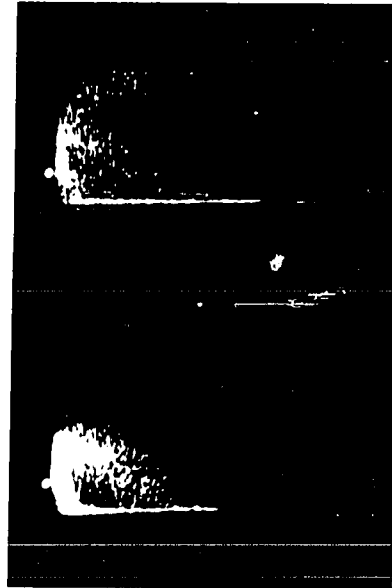
Figure 6-1

Po-Be Neutron Source
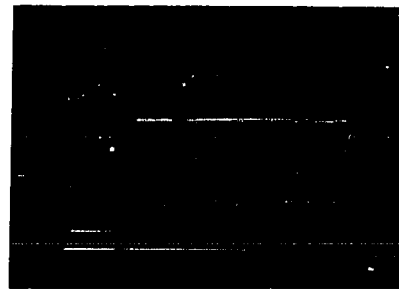
Na 22 Gamma Source

BRIGHTENING ON ALL PULSES

Extra Brightening   N2

Extra Brightening   N1

D1
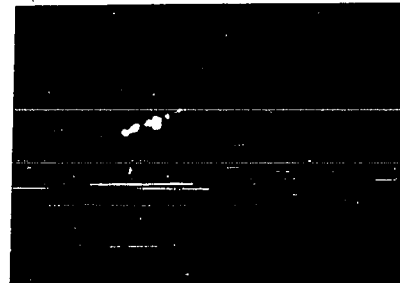
Po-Be SOURCE. BRIGHTENING SUPPRESSED

TWINKLE BOX DISPLAY
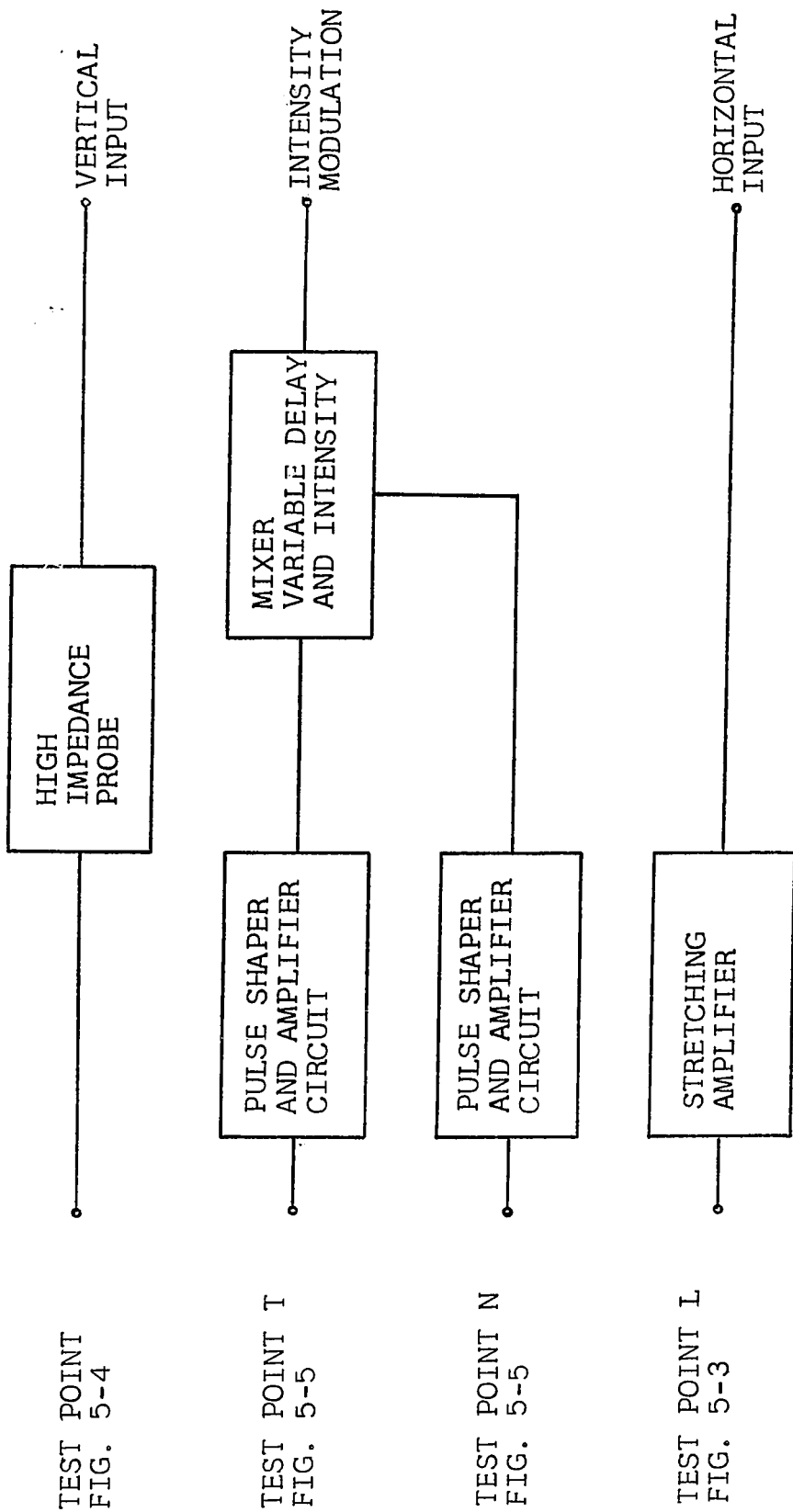
Figure 6-1

TWINKLE BOX DISPLAY SYSTEM

Figure 6-2

being 1 MeV.   Various neutron energies were obtained by exposing

the detector at 0°, 30°, 60°, and 90° to the incident deuteron

beam.   During the Van de Graaff calibrations, the spectrum from

dynode 14 was recorded in the T.M.C.P.H.A. in coincidence with

the neutron output working between the lowest and the highest

discriminators.

6.1   Rejection of Charged Particle and Gamma Ray Pulses

The theory of the pulse shape discrimination circuit network

has been given in Chapter 4.   In practice it was often difficult

to set up the final adjustment.   From the beginning the importance

of the photomultiplier stray capacitances must be appreciated, as

in the circuit the pulses are stretched on the stray capacitance.

As the required anode and dynode 13 time constants are already

determined by the requirements of Figure 5-2, it was found to be

impractical to use anything other than the smallest possible capa-

citance.   The obvious difficulty with the stray capacitance is

the variation between tubes and between mounting arrangements.

These changes in the stray capacitance must be matched by changes

in the value of R_a if the system is to operate at the required

point in Figure 5-2.   This adjustment can be a tedious procedure,

as at most the difference between a proton and electron pulse was

a 10% change as seen at point A (see Fig. 5-3).   To facilitate

this adjustment, a display system, similar to that described by

Brooks, was built. A block diagram of the display unit is shown

in Figure 6-2.   The neutron test point in the neutron amplifier

discriminator circuit is essentially an amplified and limited analog of the balance point signal. The signal from the neutron test point was impressed on the X-plates of the oscilloscope. The linear signal from dynode 14 was amplified and stretched before being applied to the Y-plates of the oscilloscope. A third pulse is taken through an emitter follower from the D 1 discriminator, amplified and shaped to a 25 Volt, 0.1 μsec pulse which is applied to the cathode of the oscilloscope. This produced the type of oscilloscope trace shown in Figure 6-1. In the final version a modification was incorporated , to allow an extra brightening of the trace when a selected coincidence circuit fired. By adjustment of the display system it was possible, not only to show the separation of the neutrons from the gamma rays, but also which pulses were being counted as neutrons by the scaler circuits.

As will be seen from Figure 6-1, the circuits discriminate the pulses into three bands. The width and separation of these bands depends strongly on two factors: -

1. The noise of the system.

2. The pulse rate.

Any noise in the system tends to spread very noticeably the width of the bands, even to the extent of completely obscuring the separation. Precautions must be taken to reduce the noise figure to as low a value as possible. The pile up of pulses at high pulse rates tends again to obscure the separation. If a second pulse occurs before the first pulse has been analysed a

PULSE HEIGHT OUT FROM NEUTRON TEST POINT.

A   B   UPPER LEVEL

NEUTRONS

NEUTRON DISCRIMINATOR

γ - RAYS

CHARGED PARTICLES

h'

TOTAL PULSE HEIGHT

DIAGRAM - 1.

A   B

COUNTS

PULSE HEIGHT

A   B

COUNTS

PULSE HEIGHT
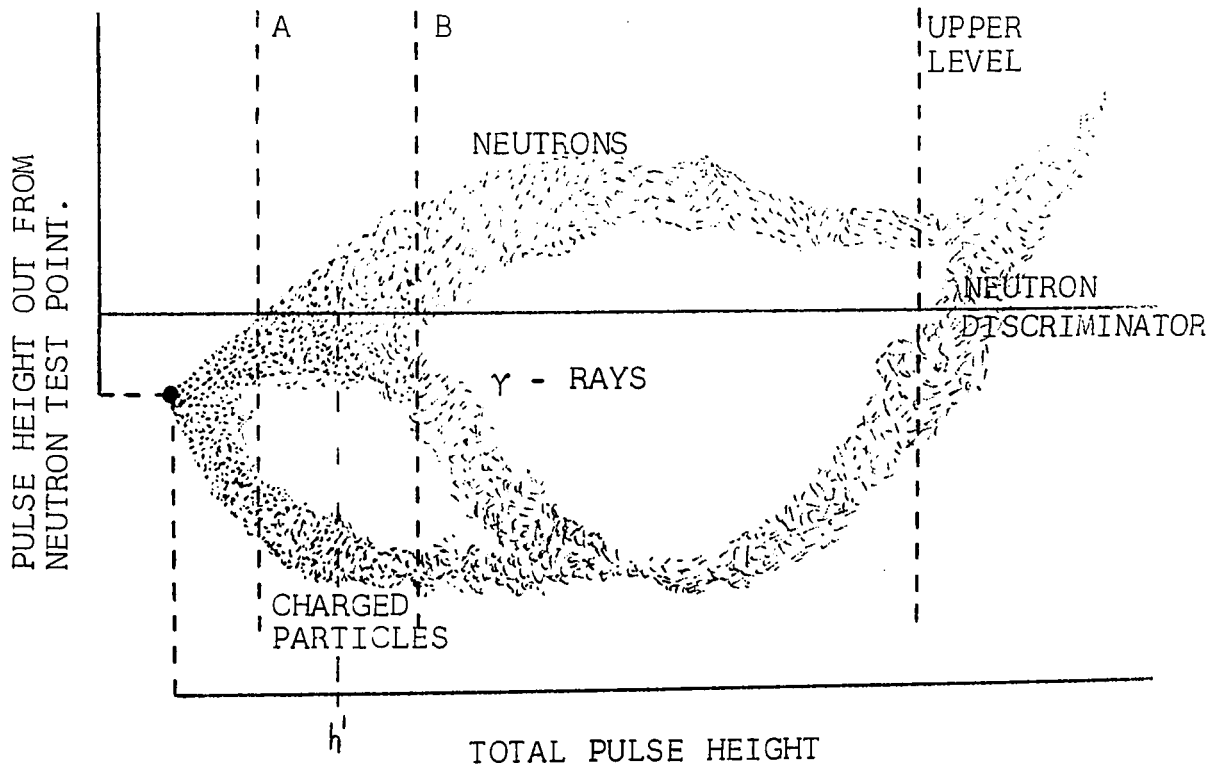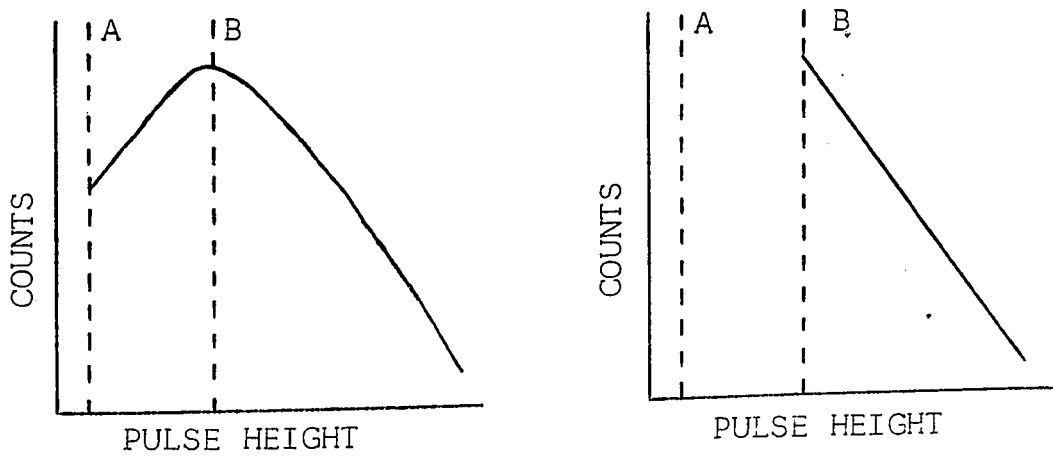
DIAGRAM - 2.

1. - SCHEMATIC DIAGRAM OF TWINKLE BOX DISPLAY SHOWING
   THE EFFECTS OF PULSE SHAPE DISCRIMINATION.
2. - EXPECTED KNOCK-ON PROTON SPECTRA FOR TWO DIFFERENT
   LEVELS OF THE LOW LEVEL DISCRIMINATOR.

Figure 6-3

spurious result will be obtained. However, with only a 10^{-3} sec resolving time and the low flux measured in the cosmic ray work, no problems were anticipated from this aspect.

A schematic drawing of Figure 6-1 is shown in Figure 6-3. It will be seen from Figure 6-3 that the loci traces are not straight lines. The distortion on the negative side is due to electronic limiting of the negative pulses in the discriminator (Figure 5-3). The consequent rise following the limiting is possibly due to a small amount of missmatch in the time constant of the dynode and anode circuits. However, this overshoot section was present to·some degree in all detectors: it may therefore be a more basic property of the system (See section on P.S.D.).

The appropriate position for the upper level and neutron discriminators are shown in Figure 6-3. The two extreme positions of the lower level discriminator are shown as A and B. If the discriminator is set at position A, the efficiency in the region of A to B is very difficult to calculate, as an unknown number of knock-on protons with pulse height h' will, due to the spread of the loci, fall below the neutron discrimination level. The spectrum produced from a power law spectrum with this setting is shown in Figure 6-3. The spectrum from the same source with setting B is also shown. In general it is more convenient to set the lower level at B than at A; however, in some of the detectors (e.g. Rig C) this was not possible due to the very large spread of the neutron trace ; in this case

the lower level was set in a position equivalent to A.

6.2 The Energy Calibration

As described previously, the neutron detector had a 3 or 4 channel pulse height analyser measuring the linear spectrum from dynode 14. For convenience the neutron channels will be referred to as N1, N2, N3, N4: N1 corresponding to the channel between D1 and D2, N2 corresponding to the channel between D2 and D3, etc. (Figure 5-1). From the Na^{22} gamma ray pulse height spectrum obtained on the T.M.C.P.H.A. and the known energy of the Compton edge, the equivalent electron energy of one of the T.M.C.P.H.A. channels can be determined. The linearity of the T.M.C.P.H.A. and the scintillator for electrons makes it possible to determine the equivalent electron energies of the other T.M.C.P.H.A. channels, and hence D1, D2, etc., using a broad spectrum gamma-ray source. Conversion to proton energies is then possible using Figure 4-4 and Equation 6.

For this method of calibration to be reliable a sensible value of kB (Equation 6) must be known. The value of kB has been determined by Birks (1951) and by Fowler and Roos (1955). Their values are 0.0091 gm/cm^2 MeV and 0.0081 gm/cm^2 MeV respectively. Fowler and Roos consider the results to be in good agreement as a value of kB depends on crystal damage and impurities. In an attempt to determine the actual response to neutrons of the detector the Van de Graaff calibration was

undertaken.

Due to detector resolution and the low energy cut-off distorting the knock-on proton spectrum, it proved quite difficult to determine the exact position of the input neutron energy on the knock-on proton spectrum. The method proposed by Batchelor et al.(1961) is to graph the integral knock-on proton spectrum and determine the position of the straight line intercept, this value being taken as the equivalent neutron energy. It was felt that this method might lead to error as the differential proton spectrum did not show a flat section as required by this method. As a check, the half height point on the fall-off, on each differential spectrum was determined, and this value taken as equivalent to the neutron energy. The results of these two methods agree in general within 10%.

As a further check on the equivalent neutron energy for the discrimination levels, the efficiency for each neutron channel was calculated using the $B^{10}F_3$ counter. The graph of efficiency versus energy for each channel should fall to zero at the neutron energy equivalent to the appropriate discrimination level. The value calculated in this way agrees in general with those previously calculated.

The light output, calculated by equation 6 with a kB value of 0.0080 gm/cm^2 MeV, versus energy is shown in Figure 4-4. The value measured by the Van de Graaff calibrations are indicated. It will be noticed that two (B and C) of the three detectors lie quite close to the theoretical curve. The deviation at the

lower energies might be expected, as the distortion from the lower level discriminator will be more pronounced at these energies. The third detector (A) is in poor agreement with the theoretical predictions. However, the curve has the same general shape as that for B and C. To fit a theoretical curve to the experimental points for detector A, the value of kB must be increased to 0.010 gm/cm^{2}MeV. This higher value of kB could be due to damage of the anthracene crystal.

In the calculation of energy response the theoretical curves shown in Figure 4-4 were used as the correct values.

6.3 The Efficiency Calibration

A definition of single scattering efficiency has been given previously (Equation 5). In this section an attempt will be made to relate the scattering efficiency to the actual detector efficiency. The scattering efficiency was derived by two different calculations; first by evaluation of equation (5), single scattering, and secondly by the Monte Carlo calculation, multiple scattering.

The scattering efficiency calculated by the Monte Carlo method is about twice as large as that derived from equation (5). The reason for this result becomes obvious when the light output spectrum from the Monte Carlo calculation is examined (Figure 6-4). It will be seen from this spectrum that almost half the counts fall into the first light output channel. These counts are from carbon collisions. As in most practical

detectors it is not convenient to detect such low light outputs, the efficiency must therefore be defined in terms of the lowest acceptable light output, i.e. the light output which gives a pulse just large enough to trigger discriminator 1.

To determine the detector efficiency, it is necessary to know the equivalent neutron energy of the low energy cut off (D1). This can be found from the previous section and will be defined as E_1. Also, each detector has an upper level energy discriminator for the 'knock-on' proton spectrum which will be defined as E_m. The detector efficiency must, by definition, be zero at E_1. For single scattering, the efficiency can therefore be defined as

$$e(E) = \frac{(E - E_1)}{E} \Sigma(E) \qquad (8)$$

in the range E_1 to E_m, where E is the neutron energy and $\Sigma(E)$ is the scattering efficiency. At energies above E_m the neutrons begin to knock-on protons, which have too high an energy to be detected, and so the efficiency becomes

$$e(E) = \frac{(E_m - E_1)}{E} \Sigma(E) \qquad (9)$$

for $E > E_m$.

Equations (8) and (9) hold only for a detector in which second scattering may be ignored. In the more general case the efficiency $\Sigma(E)$ must be determined from the Monte Carlo calculations. The output from the Monte Carlo programme is essentially a graph of the number of counts in a given light interval versus the light output. The efficiency at any energy used in
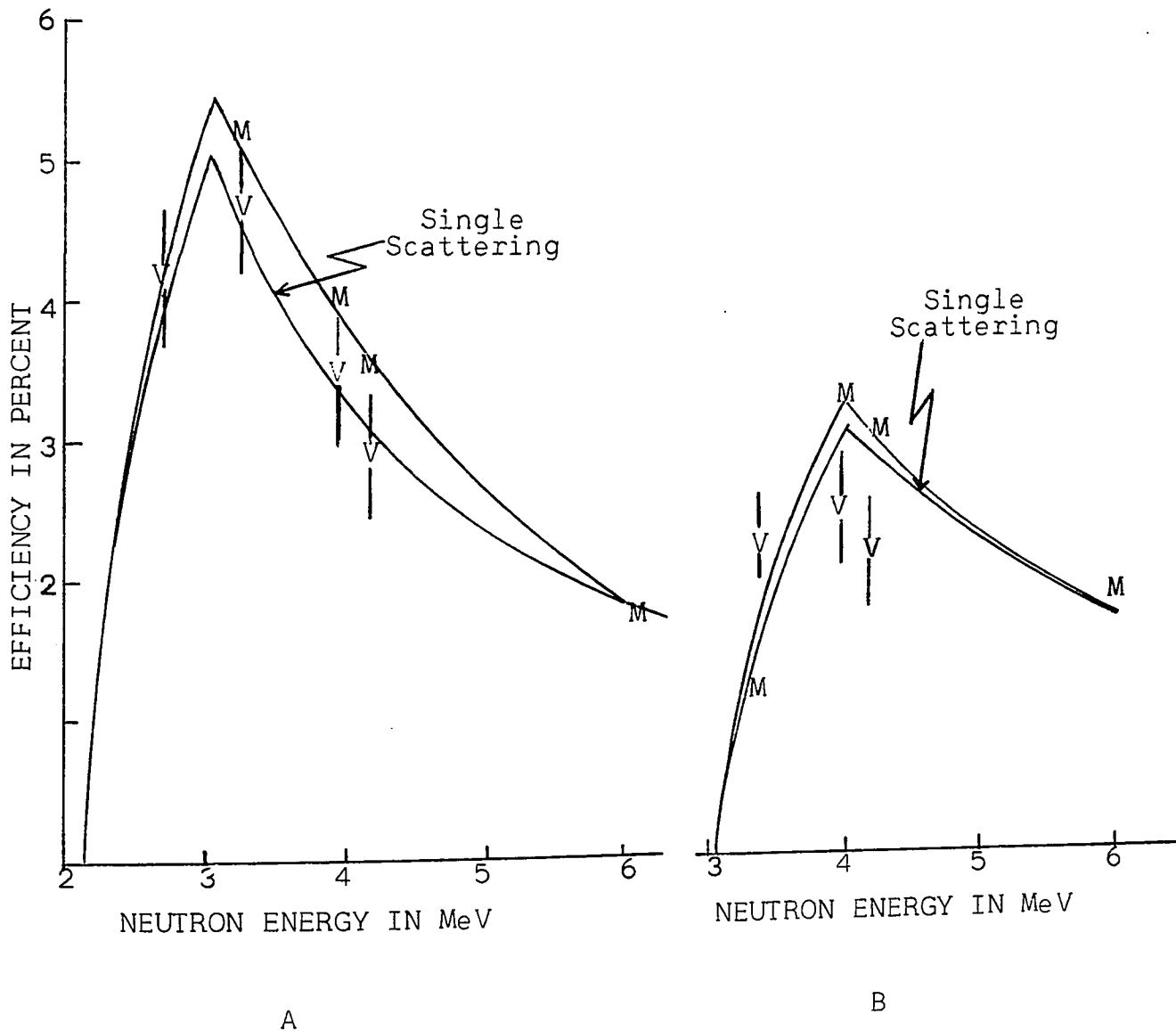
TYPICAL RESPONSE CURVES FOR THE CHANNEL (A)N1   (B)N2

V = VAN DE GRAAFF EFFICIENCY
M = MONTE CARLO EFFICIENCY

SINGLE SCATTERING EFFICIENCY IS SHOWN FOR COMPARISON

Figure 6-5

the calculations can be found from

$$e(E) = \int_{L_1}^{L_2} N(L)dL \qquad (10)$$

where L_1 and L_2 are the upper and lower lights levels respec-
tively, in terms of electron light output. The reponse curves
derived in this manner are different from the single scatter
curves for the lower energies. The disagreement is not unex-
pected, as second scattering will be much more common at lower
energies.

The reponse curves of the individual neutron channels are
shown in Figure 6-5. It will be noticed that the Monte Carlo
reponse and the single scatter reponse are significantly diff-
erent only for the N1 channel in each case. It was therefore
concluded that the single scattering curve was an adequate
approximation of channels N2, N3, and N4, but that the Monte
Carlo results should be used for N1.

The calculations of the response curves can be checked to
some extent by the results of the Van de Graaff calibration.
During each run on the Van de Graaff, the neutron flux was
measured by a standard $B^{10}F_3$ counter. This flux was corrected
for the different effective areas, distance from the source and
for the angular flux distribution. It was then compared to the
flux measured by the scintillation detector and the detector
efficiency was determined for each of the detectors. These are
shown in Figure 6-5, which includes the theoretical curve for
comparison.
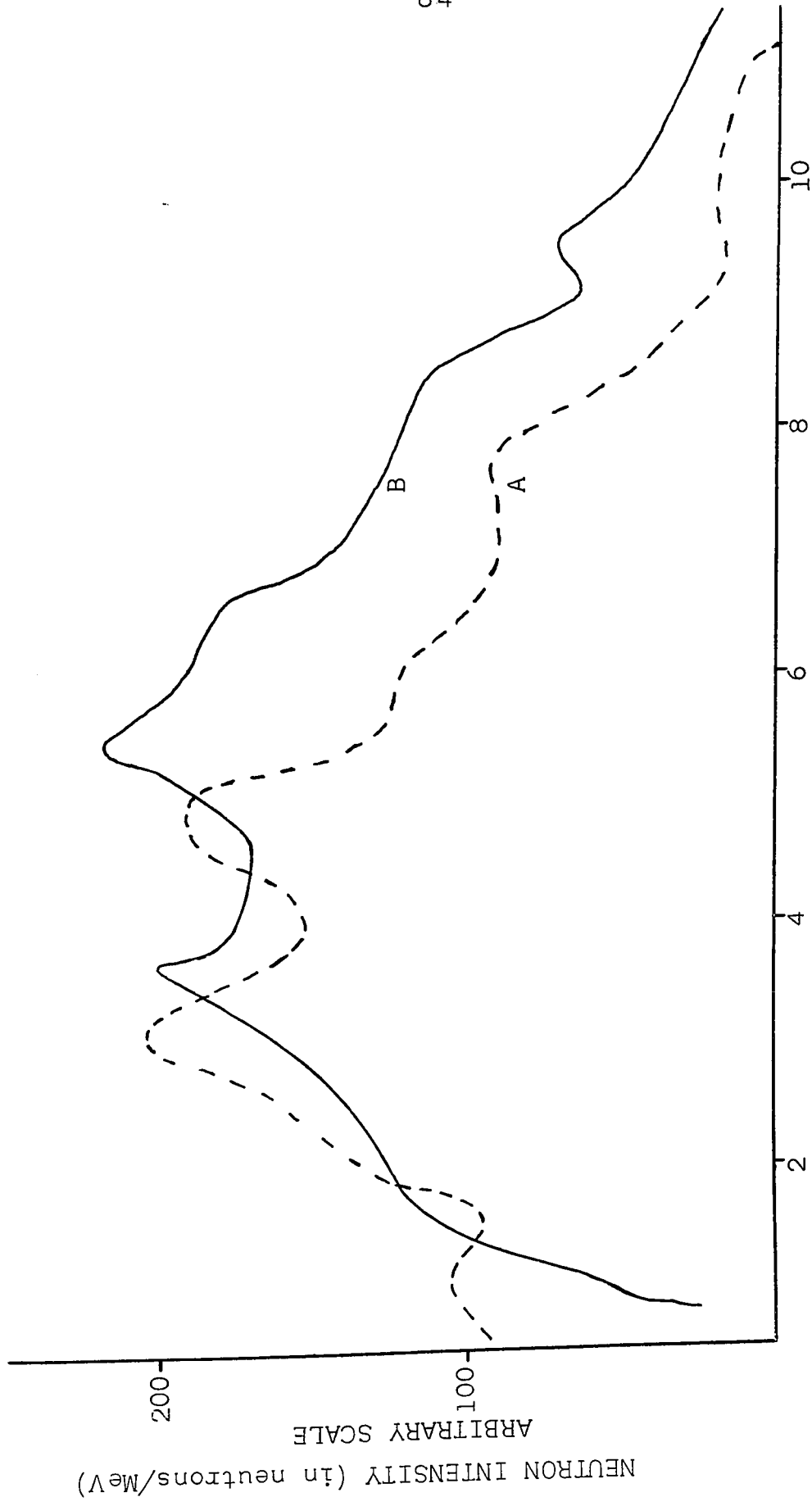
Po - Be NEUTRON SPECTRUM ACCORDING TO   A. COCHRAN AND HENRY,
                                        B. WHITMORE AND BAKER.

Figure 6-6

	Detector A	Detector B	Detector C
N1	1.21	0.87	1.80
N2	1.19	1.15	2.00
N3	0.98	1.27	2.00
N4	1.28	0.96	1.80

THE RATIOS OF THE THEORETICAL COUNT RATE
FROM THE Po-Be SOURCE TO THE OBSERVED

COUNT RATE.

Table 5.

The response curves, calculated above, were checked using the polonium-beryllium (Po-Be) neutron source. The Po-Be source was placed at a known distance from the detector and the energy spectrum measured by the T.M.C.P.H.A. Unfortunately the source spectrum for neutrons for Po-Be is not well known. The theoretical calculations of Hess (1959) agree only in general form with the experimental values of Cochran and Henry (1955), Whitmore and Baker (1960) and Medveczky (1956). Due to the relative agreement between Cochran and Henry (1955) and Whitmore and Baker (1950), above 2 MeV, an average of these two spectra was used. Assuming the spectrum of neutrons from the source, Figure 6-6, and the energy response of the detector, it is possible to integrate the spectrum graphically over the region of interest. As the source strength is known and the geometric correction can be worked out, it is possible to calculate the expected number of neutrons in each channel. The ratios of expected to the measured number are shown in Table 5.

6.4 Angular Resolution and Effective Area of the Detector

As will be seen from equation (5), the scattering efficiency of an organic scintillator for neutrons is a function of the distance 'ℓ', travelled by the particle in the scintillator. As the efficiency is relatively low and a relatively quickly varying function of ℓ, the actual cross-sectional area exposed to the neutron flux is not an accurate measure of the effective area. A better approximation is obtained from

dependent term and of an angle dependent term. In order to solve equations (12) and (13) some approximation must therefore be made.

It was noticed that to within about 20%, the effective area was a constant with angle, i.e. the detector was almost omnidirectional. It was also noted that the validity of assuming an omnidirectional detector was energy dependent. Under isotropic irradiation the average effective area, over all angles at 1.5 MeV neutron energy, was found to be 0.91 the effective area at $90°$. The equivalent factor at 6.00 MeV was found to be 0.96 and at 3 MeV to be 0.93. In order to solve equation (12) it was therefore assumed that

$$\Gamma'(E,E_1) = 0.93A(\pi/2)\Sigma(E_1,E,\pi/2)$$

This assumption is not expected to introduce any appreciable error, and certainly no error in excess of 2 or 3%.

Using this assumption equation (13) reduces to

$$\mathcal{N} = {}_{E_1}\!\int^{\infty} KE^{-x}(0.93\times12.9)\Sigma(E_i,E)dE$$

$$= 12{}_{E_1}\!\int^{\infty} KE^{-x}\Sigma(E_1,E)dE \tag{14}$$

Substituting for $\Sigma(E_1,E)$ from equation (8) and (9), one obtains

$$\mathcal{N} = 12{}_{E_1}\!\int^{E_m} KE^{-x}[(E-E_1)/E]\Sigma(E)dE \tag{15}$$

$$+ 12{}_{E_m}\!\int^{\infty} KE^{-x}[(E_1-E_m)/E]\Sigma(E)dE$$

This can be reduced to a simple equation if a simple energy dependent term is found for $\Sigma(E)$. This procedure yields results equivalent to the calculation of Broek and Anderson

(1960).

A better approximation is to integrate equation (14) numerically over the response curves for each energy channel shown in Figure 7-2.

6.5   Discussion of the Calibration

As the detectors were built at various times, the complete calibration procedure outlined was followed only for the last set of detectors, A,B,C and 6.   The other two detectors, 44 and 5, from which useful results were obtained, were calibrated in a somewhat different manner.   A further detector, 59, was calibrated in approximately the same manner as A,B,C and 6.

From the results of the complete calibration two important points emerge: -

1.   kB may be taken as 0.008 gm/cm^2-MeV for detectors B,C,6 and 59.   For A however, kB must be a somewhat higher value.

2.   The theoretical efficiency agrees with the efficiency obtained from the Van de Graaff for B and 6.

On the basis of the first point it was assumed that the value of kB for anthracene must be 0.008 gm/cm^2-MeV and that this value may be used in converting the gamma ray calibration of 44 and 5 to a knock-on proton calibration.

The interpolation of an efficiency for detectors 44 and 5 is perhaps more uncertain.   As previously stated, the Van de Graaff efficiency agrees with the theoretical efficiencies for

Energy	2.70	3.35	3.91	4.14	
N1	1.00	1.1	1.1	1.3	Detector B
N2		0.7	1.2	1.4	
Total		1.00	1.3	0.9	Detector 6
Total	2.00	1.90	2.30	2.40	Detector C

THE RATIOS OF THE THEORETICAL EFFICIENCY
TO THE VAN DE GRAAFF EFFICIENCY.

Table 6.

B and 6. However, the Van de Graaff efficiency does not agree
for detectors A or C. The efficiency results for A are diffi-
cult to understand, as they were a factor of two higher than
the theoretical at 2 MeV, but about the theoretical value at
4 MeV. Normally this would lead one to believe that the
neutron discriminator had shifted in such a manner as to count
gamma rays. This does not appear to be the case as the Po-Be
calibration, which is a gamma and neutron emitter, yielded
results consistent with the theoretical efficiency. It must
therefore be assumed that during the calibration of detector A,
the $B^{10}F_3$ counter used to monitor the neutron flux was not
working properly, and that the efficiency of A was close to the
theoretical efficiency.

The discrepancy between theoretical and experimental eff-
iciencies for detector C can be traced to the detector (Table 6).
Detector C was known to be a noisier system than usual. This
was probably due to the photomultiplier tube. For this reason
the neutron discriminator had to be set much higher than usual
and hence it is probable that some of the neutron counts were
lost below the discriminator level. The results of the Van de
Graaff calibration are consistent with the efficiency from the
Po-Be source. Hence the theoretical efficiencies were normal-
ized down to the Van de Graaff efficiencies.

The interpolation of the efficiencies of 44 and 5 must be
considered in the light of the above discussion. It is known
from the photographs of the loci, obtained while setting up the

N.R.C. Black Brant Rocket Code Number	Neutron Detector	Date	Flight Time in sec	Apogee in Km	Rocket Performance	Detector Live-Time in sec	Detector Performance
		1964					
AA-II-41	41	8 Jan	337	115	High lateral G at burnout	~ 300	Neutron detector worked throughout flight. Data appears unreliable. Spurious 'burst counts'.
AA-II-44	44	9 April	373	154	Good	~ 350	Good
AA-II-36	36	17 April	373	152	Good	~ 80	High voltage batteries failed at T plus 85 sec.
AK-II-59	59	8 Sept	15	---	Nose cone parted from rocket at T plus 15 sec	0	No data
		1965					
AA-II-53	B	24 March	390	166	Good	~ 370	Good
AA-II-60	A	24 March	375	155	Good	~ 350	Lost data from neutron channel N3. Otherwise good.

ALL OF THE ABOVE ROCKET FLIGHTS WERE MADE FROM FORT CHURCHILL, MANITOBA

Table 7

95

Neutron Detector	Location	Date	Time	Detector Lifetime in hrs	Remarks
Eclipse	Ft Providence, N.W.T.	20 July 1963	Day	0	Rig failed shorly after launch due to radio-frequency problems.
Rig 5	Ft Churchill, Manitoba	17 April 1964	Night	1	Intermittant H.V. corona at 75 Kft.
Rig C	Ft Churchill, Manitoba	27 March 1965	Day	1	Apparent continuous corona at 80 Kft.
Rig 6	Ft Churchill, Manitoba	1 April 1965	Day	3.5	Failure at launch. Gamma ray data only received throughout flight.

REVIEW OF DETECTOR PERFORMANCE

Table 7 (cont'd)

FLIGHT TIME (SEC.)

HEIGHT (Thousand Feet).
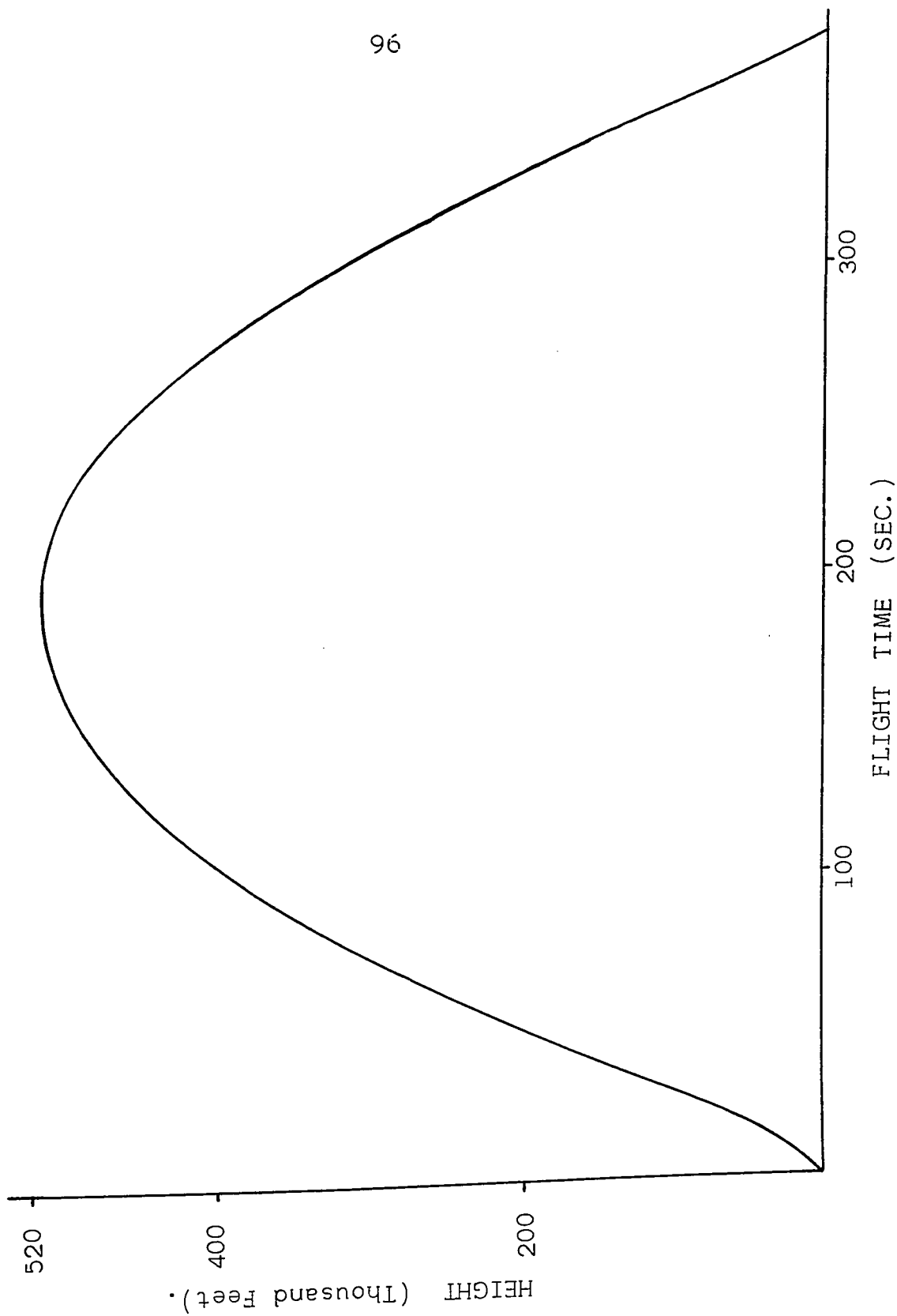
RADAR PLOT OF ROCKET TRAJECTORY FOR AA-II-60.

Figure 7-1

EQUIVALENT PROTON ENERGY

	AA-II-44	Rig B AA-II-53	Rig A AA-II-60
D1	2.70 ± 0.05	2.15 ± 0.05	1.73 ± 0.10
D2	3.10 ± 0.10	3.05 ± 0.05	2.90 ± 0.10
D3	5.4 ± 0.20	3.90 ± 0.05	5.55 ± 0.20
D4	10.0 ± 0.30	4.85 ± 0.05	8.10 ± 0.20

	ΔE*	E**	ΔE*	E**	ΔE*	E**
N1	0.4	2.90	0.90±0.1	2.60	1.17±0.2	2.32
N2	2.3	4.25	0.85±0.1	3.48	2.65±0.3	4.23
N3	4.6	7.70	0.95±0.1	4.37	2.55±0.4	6.83
N4	---	----	1.25±0.2	5.48	1.20±0.4	8.70

* ΔE - width of channel in p^+MeV
** E - center energy in p^+MeV

CALIBRATION DATA - ROCKET BORNE DETECTORS

Table 8

	AD-II-44 counts/min	AA-II-53 counts/min	AA-II-60 counts/min
N1	6.0	10.9	16.4
N2	13.1	9.4	24.2
N3	9.25	6.7	----
N4	-----	8.7	3.1

|	counts/min-MeV	counts/min-MeV	counts/min-MeV
N1	15	12.1	14.0
N2	5.7	11.1	9.2
N3	2.0	7.1	----
N4	----	7.0	2.6

ROCKET RESULTS

Table 9

While the rocket borne detectors performed reasonably satisfactorily, the balloon borne packages were all at best partial failures. The eclipse flight failed due to radio frequency bias on the tunnel diode discriminators, which led to the shifting of some or all of the calibration levels. The count rate was therefore tens of times higher than expected. In all subsequent detectors a radio frequency choke was placed in series with all tunnel diodes. This precaution, along with a redesigned transmitting antenna, effectively eliminated the radio frequency problem. The balloon detectors 5 and C failed due to corona discharge. The precautions taken to prevent corona have been outlined previously. Detector 6 failed shortly after launch: probably due to a poor connector in the neutron circuit.

Useful results then were obtained from rockets AD-II-44, AA-II-53, and AA-II-60. Data were used from launch time plus 60 seconds to impact time minus 60 seconds approximately, for each flight. During this time interval the rocket was above 200,000 feet (Fig. 7-1). Due to the small count rate no noticeable change in the count rate is expected between 200,000 feet and apogee.

Useful data were obtained from the balloon borne detectors 5 and C up to about 70,000 feet or 100 gm/cm^2.

7.1 Rocket Results

Tables 8 and 9 show calibration data and experimental results for the three successful rocket borne detectors. Figure
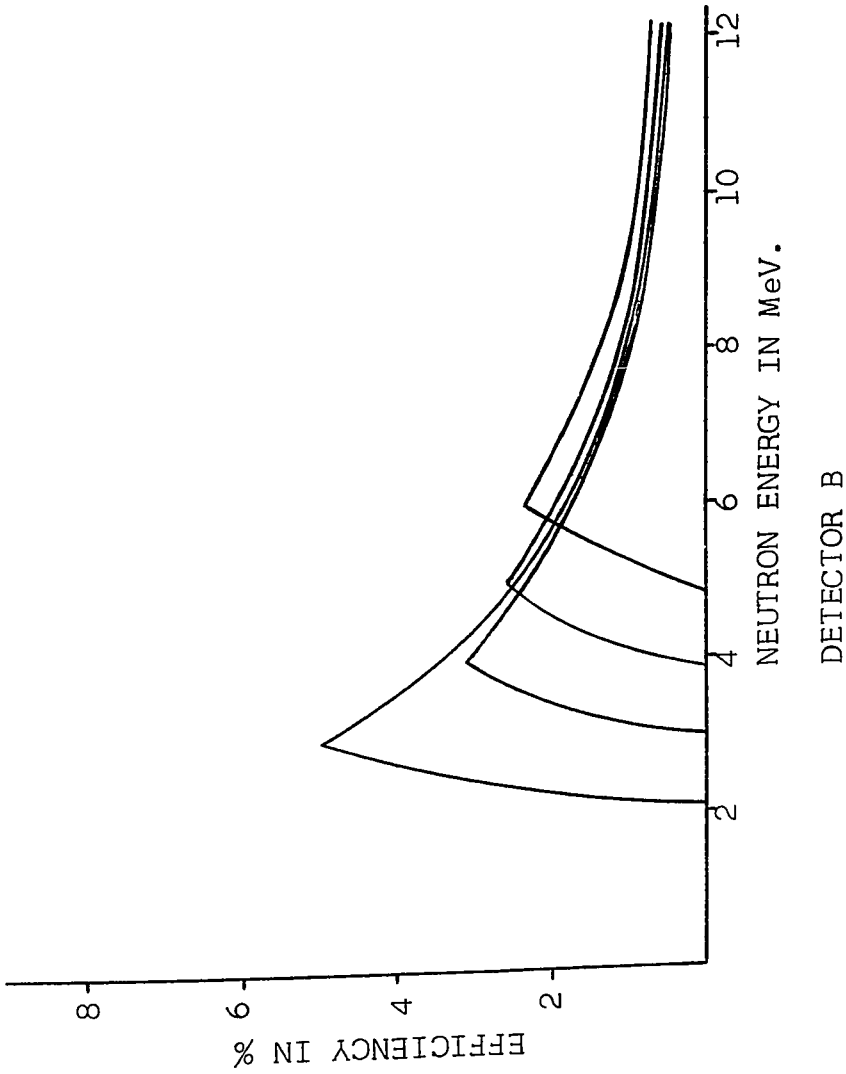
NEUTRON ENERGY IN MeV.

DETECTOR B

THE EFFICIENCY RESPONSE CURVES AS A FUNCTION OF
ENERGY FOR THE VARIOUS NEUTRON CHANNELS.
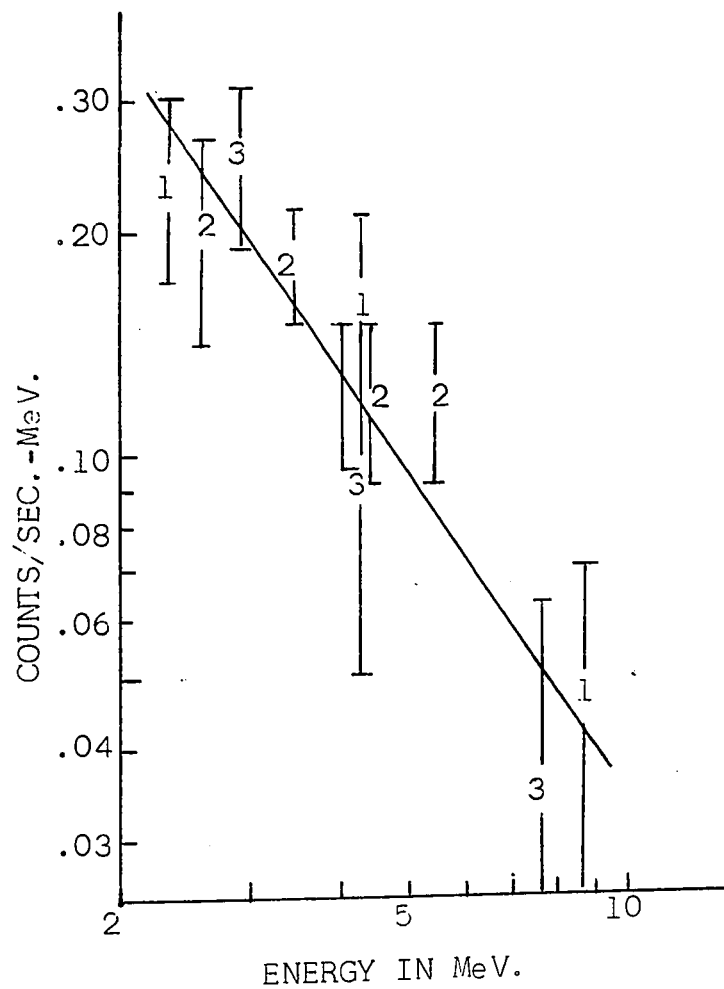
Figure 7-2(b)

KNOCK – ON PROTON SPECTRUM (ROCKETS)

1. ROCKET AA-II-60 – DETECTOR A

2. ROCKET AA-II-53 – DETECTOR B

3. ROCKET AA-II-41 – DETECTOR 44

Figure 7-3

change between the flights; hence the knock-on proton spectrum

was derived on the basis of assuming the spectrum for all three

flights was the same.

The knock-on proton spectrum derived from these results

may be given by

$$\frac{dN_p}{dE_p} = 59.7 \; E^{-1.48 \pm 0.2} \; \text{protons/min-MeV}$$

Using the known values for $\sigma(E)$ (Gammel, 1963, and following

the calculation of Broek and Anderson (1960), the incident neut-

ron spectrum, obtained from the rocket measurements, is given by

$$\frac{dN_n}{dE_n} = 0.29 \; E^{-0.85 \pm 0.30} \; \text{neutrons/MeV-cm}^2\text{-sec}$$

The spectrum determined by use of the response curves is

given by

$$\frac{dN_n}{dE_n} = 0.30 \pm 0.06 \; E^{-0.72 \pm 0.30} \; \text{neutrons/MeV-cm}^2\text{-sec}$$

The errors quoted in the above exponent allow for the error

in the determination of the channel widths used to derive the

proton spectra and the statistical errors in the count rate,

but do not include any errors involved in the efficiency cali-

bration. The error in the coefficient allows for a 20% error in

the efficiency.

7.2 Balloon Results

The useful balloon data were severely restricted. For

detectors 5 and C results were obtained from launch to about

100 mb. The onset of corona was noticed as an appreciable

NEUTRON ENERGY IN MeV.
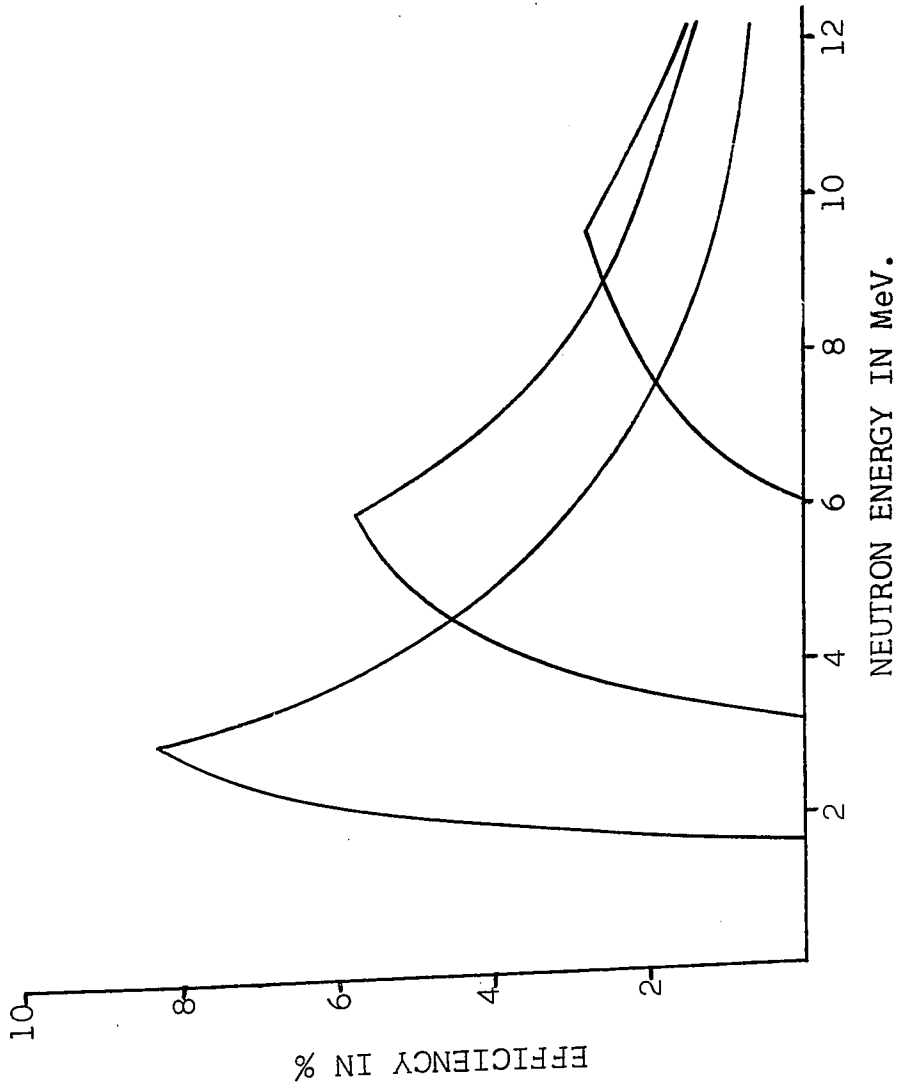
DETECTOR 5

THE EFFICIENCY RESPONSE CURVES AS A FUNCTION OF
ENERGY FOR THE VARIOUS NEUTRON CHANNELS.

Figure 7-4(a)
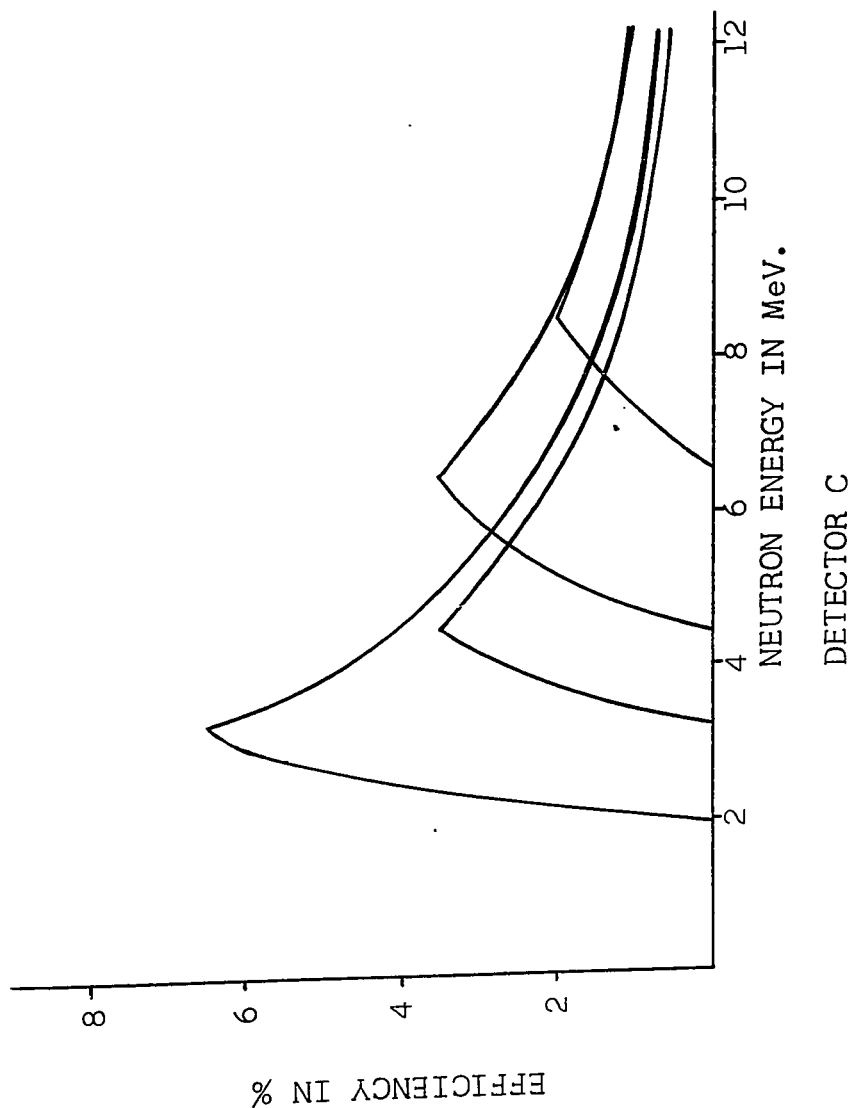
NEUTRON ENERGY IN MeV.

DETECTOR C

THE EFFICIENCY RESPONSE CURVES AS A FUNCTION OF
ENERGY FOR THE VARIOUS NEUTRON CHANNELS.

Figure 7-4(b)

EFFICIENCY IN %
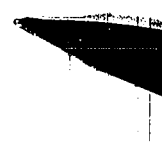
EQUIVALENT PROTON ENERGY

	Balloon Rig 5	Balloon Rig C
D1	1.61	1.95
D2	3.12	3.25
D3	6.05	4.40
D4	9.60	6.50
D5		8.55

	Channel Width in p+MeV	Center Energy in p+MeV	Channel Width in p+MeV	Center Energy in p+MeV
N1	1.51	2.37	1.30	2.60
N2	2.93	4.59	1.15	3.87
N3	3.55	7.83	2.10	5.45
N4			2.05	7.57

CALIBRATION DATA - BALLOON BORNE DETECTORS

Table 10
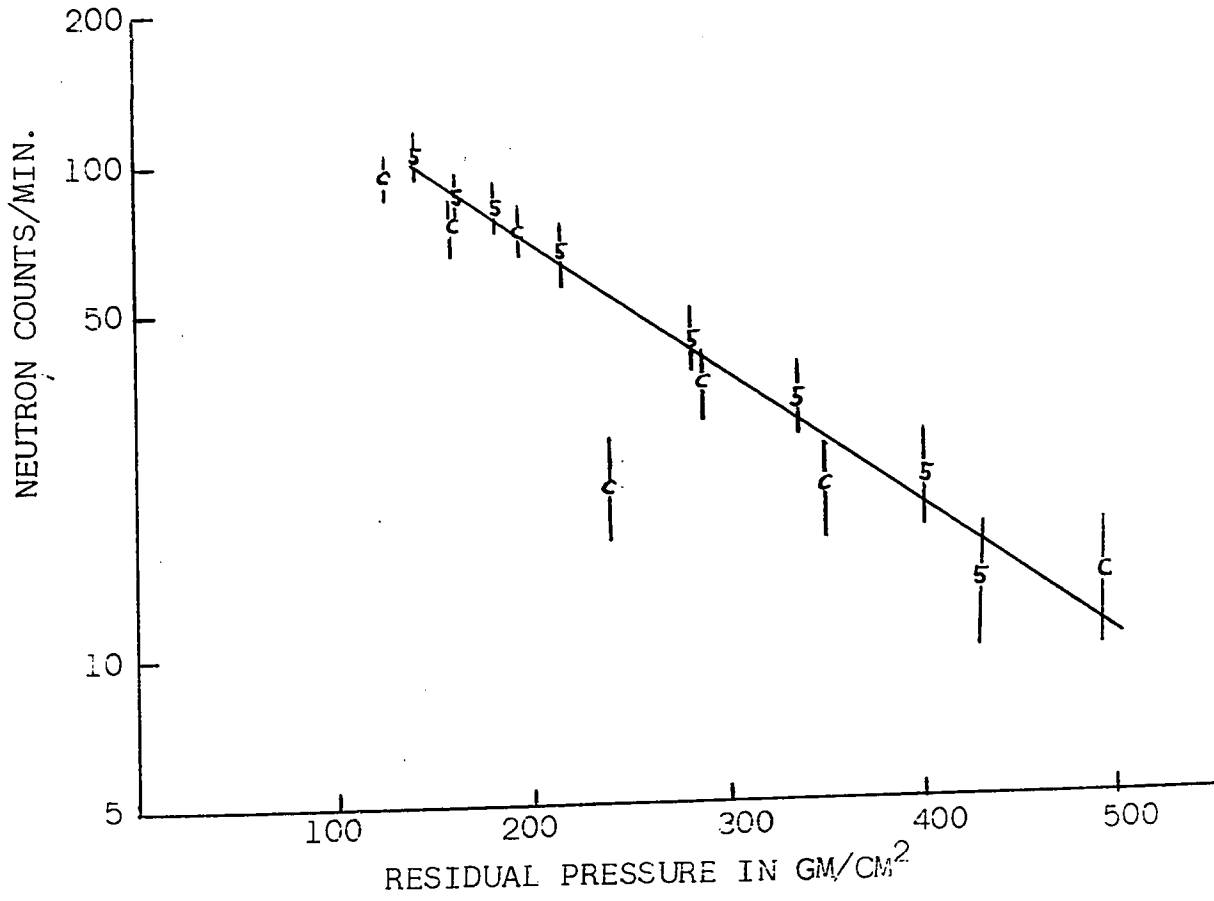
NEUTRON COUNT RATE AS A FUNCTION OF ALTITUDE FOR
BALLOON BORNE DETECTOR 5 AND C.

Figure 7-5
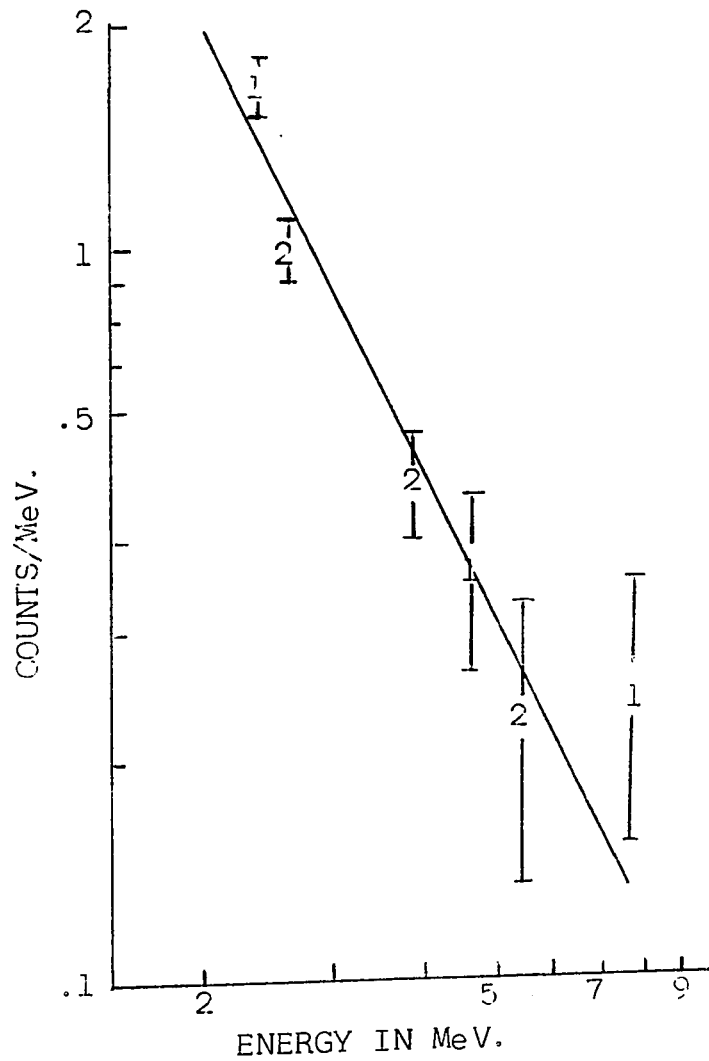
KNOCK - ON   PROTON   SPECTRUM. (BALLOONS)

1.   BALLOON 17 APRIL, 1964 - DETECTOR 5

2.   BALLOON 27 APRIL, 1963 - DETECTOR C

THE COUNTS/MeV. ARE PLOTTED ON

AN ARBITRARY SCALE.

Figure 7-6

$$\frac{dN_p}{dE_p} = K \, E^{-2.00 \, \pm \, 0.2} \text{ protons/min-MeV}$$

where K is a constant.

An altitude dependence of

$$21 \exp (-0.0068 \pm 0.0009 \, P) \text{ protons/min-cm}^2$$

and $\quad 15 \exp (-0.0055 \pm 0.0011 \, P) \text{ protons/min-cm}^2$

was found for detectors 5 and C respectively, where P is the residual pressure in gm/cm^2. These latter values lead to an average mean free path for absorption of $154 \pm 17 \text{ gm/cm}^2$.

Following the calculations of Broek and Anderson (1960) this yields a neutron spectrum of

$$\frac{dN_n}{dE_n} = K \exp (-P/154 \pm 17) \, E^{-1.35 \, \pm \, 0.3} \text{ neutrons/sec-cm}^2\text{-MeV}$$

The spectrum determined using the response curves is given by

$$\frac{dN_n}{dE_n} = K \exp (-P/154 \pm 17) \, E^{-1.42 \, \pm \, 0.3} \text{ neutrons/sec-cm}^2\text{-MeV}$$

The errors quoted in the above equations allow for statistical errors, the errors in the channel widths but not for any error caused by the normalization.

7.3 Gamma Ray Results

As previously mentioned, the gamma ray data was used mainly as a check system. The data from all the flights were scanned to see if there were any sudden changes in count rate and to make sure that the incident flux was at an acceptable value. Except where previously noted no unusual gamma rates occurred.

As the detector was not calibrated in terms of efficiency for gamma rays, nothing can be said about the absolute flux. However, the mean free path for absorption can be calculated for gamma rays in the energy range 0.5 MeV to 5 MeV. The mean free path obtained from detectors 5 and 6 yield an average value of 146 $\pm$ 20 gm/cm^2.

to assume that this shape is a constant feature. These assumptions are open to question. Recently Boella et al (1965) have shown that the leakage spectrum appears latitude dependent. It is therefore important to determine not only the flux, but also the spectrum as functions of both latitude and altitude.

To determine both the flux and energy spectrum of cosmic ray neutrons is not a simple problem. The organic scintillator pulse shape discrimination detectors used by Haymes (1964), Mendell and Korff (1963) and the author, are all of limited energy range and it seems unlikely (Chapter 4) that this range can be extended much further. The accuracy of the spectrum and flux derived from these experiments is limited, not only by the count-rate, but also by the resolution function of the detector arrangements which has not been taken into account by any of these authors. Notwithstanding, these experiments probably give the best estimates of the flux and energy spectrum available at this time.

The determination of the spectra at higher (> 10 MeV) and lower (< 1 MeV) energies presents a more difficult problem as at present no really suitable techniques are available. The technique developed by Bramblett et al (1960) for the lower energies, while a useful laboratory method, is difficult to use in rockets or balloons as several detectors have to be flown simultaneously.

8.2 Discussion of the Present Results

The flux and energy spectrum for neutrons above the atmosphere has been determined in the energy range 2 to 10 MeV at a

geomagnetic latitude of 68.8°N.

The exponent of the energy spectrum above the atmosphere, - 0.7 ± 0.3, is smaller than the previously published measurements of - 1.3 ± 0.1 at 41°N (Haymes, 1964) and - 1.16 ± 0.2 at 53°N (Mendell and Korff, 1963), obtained at balloon altitudes of 4 and 10 gm/cm² residual pressure respectively. It will be noted that these measurements were obtained at both lower latitude and lower altitude. The change in the spectrum, if real, may therefore be due to either a latitude or altitude effect. It is unlikely that either local production or absorption in the rocket can account for such a change in the spectrum (Appendix 1).

The recent results of Boella et al (1965) suggest that there may be a spectral change, at high altitude, with latitude. They suggest that the spectrum at high latitudes is flatter, (i.e. a lower value of the exponent) than previously expected. The present results confirm this. However, the calculations of Newkirk (1963) show a leakage spectrum which is flatter than the spectrum measured in the atmosphere. It is not possible , therefore, with these results to decide if the spectral change is an altitude or latitude effect, or a combination of the two.

The exponent of the spectrum, - 1.4 ± 0.3, determined low in the atmosphere,agrees, within the limits of error, with the values of Haymes and of Mendell and Korff, who found a constant exponent up to ceiling altitude.

The total leakage value between 1 and 10 MeV may be compared

with the data of Haymes extrapolated to the top of the atmos-
phere. The flux as measured with an omnidirectional detector at
0 gm/cm^2, estimated by Haymes at 41°N, is 0.24 neutrons/cm^2-sec;
the value determined by this experiment at 0.1 gm/cm^2 and 68.8°N
is 1.0 $\pm$ 0.4 neutrons/cm^2-sec. The latitude variation for these
two latitudes, predicted by Lingenfelter at solar minimum is
about 4.1. The measured variation is 4.1 $\pm$ 1.6. The agreement
is therefore good. However, the extrapolation of the balloon
data from even 4 gm/cm^2 to the top of the atmosphere is not a
simple problem. The very good agreement in the latitude effect
is therefore probably fortuitous. It is also important to
remember that the present results indicate a larger spectral
change than predicted by Lingenfelter, and in any discussion of
the latitude variation the effect of such a spectral change
must be considered.

8.3 Conclusion

The neutron energy spectrum at geomagnetic latitude 68.8°N
and at altitudes greater than 200,000 feet has been determined
as

$$\frac{dN_n}{dE_n} = 0.30 \pm 0.06 \; E^{-0.70 \pm 0.30} \; \text{neutrons/MeV-cm}^2\text{-sec.}$$

in the energy range 1 to 10 MeV.

The neutron energy spectrum at 68.8°N, deep in the atmos-
phere has the form

$$\frac{dN_n}{dE_n} = K \exp(-P/154 \pm 17) \; E^{-1.42 \pm 0.3} \; \text{neutrons/sec-cm}^2\text{-MeV}$$

Gauger, J., 1965, J. Geophys. Res., 70, 3571.

Gervais de Lafound, Y. and Bouyssou, J., 1963, Nuclear Instr. and Methods, 22, 365.

Gibbons, P.E., Northrop, D.C. and Simpson, O., 1961, Proc. Phys. Soc. London, 79, 373.

Greenhill, J.G., Phillips, J., Fenton, K.B., Fenton, A.G. and Bowthorpe, M., 1965, paper presented at International Conference on Cosmic Rays, London.

Gross, E., 1956, quoted by Lingenfelter, R.E., 1963, Rev. Geophys., 1, 35.

Haymes, R.C., 1959, Phys. Rev., 116, 1231.

Haymes, R.C., 1964, J. Geophys. Res., 69, 853.

Haymes, R.C., 1965, Rev. Geophys., 3, 345.

Hess, W.N., 1959, Ann. Phys., 6, 115.

Hess, W.N., Canfield, E.H. and Lingenfelter, R.E., 1961, J. Geophys. Res., 66, 665.

Hess, W.N., Patterson, H.W., Wallace, R. and Chupp, E.L., 1959, Phys. Rev., 116, 445.

Hess, W.N. and Starnes, A.J., 1960, Phys. Rev. Letters, 5, 48.

Kalos, M. and Goldstein, H., 1956, Nuclear Development Corporation of America, Report No. NDA 12-16.

Korff, S.A. and Haymes, R.C., 1960, J. Geophys. Res., 65, 3163.

LeCouteur, K.J., 1952, Proc. Phys. Soc. London, 65, 718.

Lenchek, A.M., and Singer, S.F., 1963, Planet. Space Sci., 11, 1151.

Lingenfelter, R.E., 1963, J. Geophys. Res., 68, 5633. Also 1963, Rev. Geophys., 1, 35.

Lockwood, J.A., Friling, L. and Wilson, T.,1965, paper presented at International Conference on Cosmic Rays, London.

Lord, J.J., 1951, Phys. Rev., 81, 901.

Martin, J.P., 1965, J. Geophys. Res., 70, 2057.

Martin, J.P., Witten, L. and Katz, L., 1963, I.E.E.E. Trans. N.S., 10, 1, 12.

Medvecsky, L.L., 1956, quoted in 'Fast Neutron Physics', ed. Marion, J.B. and Fowler, J.L., Interscience Publishers.

Mendell, R.B. and Korff, S.A., 1963, J. Geophys. Res., 68, 5487.

Metropolis, N., Bivins, R., Storm, M., Turkevich, A., Miller, J.M. and Friedlander, G., 1958, Phys. Rev., 110, 185.

Miles, R.F., 1964, J. Geophys. Res., 69, 1277.

Miyake, S., Hinotani, K. and Nunogaki, K., 1957, J. Phys. Soc. (Japan), 12, 113.

Neher, H.V. and Anderson, H.R., 1962, J. Geophys. Res., 67, 1309.

Newkirk, L.L., 1963, J. Geophys. Res., 68, 1825.

Owen, R.B., 1958, I.R.E. Trans., N.S. 3, 189.

Owen, R.B., 1962, I.R.E. Trans., N.S. 9, 285.

Parsons, N.R., Greenhill, J.G., Fenton, K.B. and Fenton, A.G., 1963, Proc. International Conference on Cosmic Rays, Jaipur, 2, 38.

Pomerantz, M.A. and Agarwall, S.P., 1962, Phil Mag., 7, 1503.

Prescott, J.R., 1961, Private Communication.

Reid, W.B. and Hummel, R.H., March, 1963, Nuclear Enterprises, Internal Report, Winnipeg, Canada.

Rose, D.C., Fenton, K.B., Katzman, J. and Simpson, J.A., 1956, Can. J. Phys., 34, 968.

Sandström, A.E., Pomerantz, M.A. and Gronkvist, B., 1962, Tellus, 14, 356.

Simpson, J.A., 1951, Phys. Rev., 83, 1175.

Singer, S.F., 1958, Phys. Rev. Letters, 1, 181.

Soberman, R.K., 1956, Phys. Rev., 90, 934.

Suhami, A. and Ophir, D., 1964, Nuclear Instr. and Methods, 30, 141.

Trainor, J.H. and Lockwood, J.A., 1964, J. Geophys. Res., 69, 3115.

Van Allen, J.A., 1958, quoted in Van Allen, J.A. and Frank, L.A., 1959, Nature, 183, 430.

122

Walter, G. and Coche, A., 1962, Nuclear Instr. and Methods, <u>23</u>, 147.

Walter, G., Laustriat, G. and Coche, A., 1963, Private Communication.

Webber, W.R. and McDonald, F.B., 1964, J. Geophys. Res., <u>69</u>, 3096.

Wentworth, R.C. and Singer, S.F., 1955, Phys. Rev., <u>98</u>, 1546.

Whaling, W., 1958, Handbuch der Physik, <u>34</u>, 193, Springer - Verlag.

Whitmore, B.G. and Baker, W.B., 1950, Phys. Rev., <u>78</u>, 799.

Williams, R.W., 1955, Phys. Rev., <u>98</u>, 1393.

Williams, R.W. and Bostrom, C.O., 1964, J. Geophys. Res., <u>69</u>, 377.

Wright, G.T. 1956, Proc. Phys. Soc. London, <u>69</u>, 358.

Yuan, L.C.L., 1951, Phys. Rev., <u>86</u>, 128.

APPENDIX 1

LOCAL PRODUCTION AND ABSORPTION IN THE ROCKET NOSECONE

It has been pointed out by Trainor and Lockwood (1964) and by the data of Martin et al (1963) that in any attempt to measure the neutron flux at high altitude local production of neutrons due to the interaction of high energy protons with the massive material near the detector must be taken into account. Trainor and Lockwood (1964) in an appendix to their paper, outline a method of calculating this production and it is basically this method which will be followed here.

The mounting arrangement for the rocket borne detectors is shown in Figure 5-8. Just below the heat shield and approximately 10 inches below the scintillator a four inch polyurethane absorber was inserted. This was intended to thermalize the neutrons produced below the detector, especially those produced in the motor and the forward body of the rocket. It is obvious that while this absorber will remove most of the neutrons produced in the motor, it will produce a background of its own. However, the detector only subtends an angle of 0.79 steradians at the polyurethane, and while this fraction of the total production is not negligible, to a sufficient approximation it should be possible to assume an isotropic distribution of local production round the detector: i.e. ignore the difference between the polyurethane production and the production in the skin.

The material most likely to produce neutrons under proton

bombardment is the rocket skin. The chemical composition of the skin is given in Table 11. The density of the skin was 1.86 gm/cm^3 and the thickness 1.02 cm. The skin is therefore equivalent to 1.90 gm/cm^2. The material in the foam heat shield amounts to about 0.3 gm/cm^2, assuming a constant thickness of 2.54 cm. The total amount of material around the detector was therefore approximately 2.2 gm/cm^2.

In order to determine the local neutron production it is necessary to know the interaction mean free path for the primary protons. This has been evaluated by Williams (1955) for machine energies and by several authors for primary cosmic rays, principally at air shower energies. An average acceptable value for the lower energy protons appears to be about 70 gm/cm^2. From this and knowing the amount of material around the detector it is possible to find the percentage of protons which interact in the skin.

The next step is to determine the average number produced in each interaction. As mentioned previously there are two types of particles emitted from a high energy interaction, prompt and evaporation. The contribution of both these processes will be discussed. The data of Metropolis et al (1958) is perhaps the most useful in attempting to evaluate these contributions. Metropolis et al (1958) calculated the average number of prompt particles emitted from various nuclei under proton bombardment at various energies. Assuming an average primary particle energy of 2 GeV (Trainor and Lockwood, 1964) the average number of

prompt nucleons emitted from Aluminium, atomic mass 26.98 A.M.U. is approximately 6.5. As the number of nucleons emitted is not very dependent on the atomic weight this value was also used for Magnesium, atomic mass 24.3 A.M.U. It is also predicted that the ratio of neutron emission to proton emission for Aluminium, excited by a 2 GeV proton, will be 0.92. The average neutron emission is therefore 3.1 neutrons/interaction. Metropolis et al (1958) also show that the average excitation of the residual nucleus is about 75 MeV for Aluminium. In order to estimate the number of evaporation particles due to this excitation it is necessary to use the data of Dostrovsky et al (1958). Unfortunately their data was obtained for Copper (64), Gold (109) and Tantallum (181), all of which are much more massive than Magnesium. Any attempt to extrapolate these readings must lead to large errors. However, by extrapolation of the data at 200 MeV excitation an upper limit of 0.5 evaporation neutrons/interaction was obtained.

The total number of neutrons produced by interaction of a 2 GeV proton with Aluminium is therefore approximately 3.6. This value agrees quite well with an extrapolation of the values by Lenchek and Singer (1963).

The number of protons, with energy greater than 200 MeV above Fort Churchill in April 1965 has been measured by Jenkins (private communication). These results yield a value of 0.2 ± 0.02 protons/cm^2-steradian-sec.

The shape of the nose cone makes a complete integration over

all angles difficult. To put an upper limit on the local pro-
duction it was assumed that the rocket skin could be approximated
by a spherical surface of radius 5.08 cm, completely surrounding
a detector of surface area 12 cm^2.

Using the above extrapolations and assumptions, an estimate
of the upper limit for the local production of 1.30 neutrons/sec
incident on the detector, can be made. This value is approximately
15% of the free space value estimated by this experiment.

The absorption of neutrons in the rocket skin must, however,
also be considered. The total neutron cross-section for Aluminium
at 14 MeV is about 2.0 barns. Using the density and thickness
of the skin, this gives a value of about 9% for the number of
neutrons lost to the beam.

Account should also be taken of the increased absorption of
the polyurethane shield. This will not only effectively remove
the evaporation neutrons produced in the motor but also any
genuine neutrons coming from that direction. The flux is there-
fore further reduced by about a further 6%. The total losses
from the beam are therefore about 15%.

The net result therefore of considering both local produc-
tion and absorption leaves the flux values unchanged. This es-
timate is obviously not rigorous, but it appears unlikely that
local effect can account for more than about 5% of the detected
neutrons. This is a small correction when the total errors
are considered and it is not expected to materially affect the
results.

APPENDIX 2

FUTURE SUGGESTED MODIFICATIONS FOR P.S.D. DETECTOR

It has been pointed out that there is still a need for accurate and reliable data in this field. The author would like therefore to outline his ideas on the future modifications that should be incorporated in a detector of the type described in this thesis. It is obvious that to reduce the statistical error a larger detector should be built. It should preferably be flown in a rocket which has a long flight time. As anthracene is difficult to obtain in much larger crystal sizes, it may be necessary to substitute stilbene or a bubble free liquid scintillator.

To improve the reliability of the results it is suggested that an 'in flight' calibration be incorporated. This could be done fairly simply with a low power high energy α-particle source. It is felt that the data retrieval system could be greatly improved by using pulse code modulation (P.C.M.). It should be relatively simple to transmit both the P.S.D. output and the pulse height. These pulses could then be displayed in a three dimensional array to determine not only the neutron count rate but also the gamma ray-charged particle rejection at any energy. This use of P.C.M. would lead to much more reliable data as any drift or increase in noise need not lead to the loss of data as most of the analysis would be carried out on the ground and not in the rocket as at present.